THE UNIVERSITY
OF MICHIGAN
APR 25 1960
ENGINEERING
LIBRARY

The Canadian Journal of Chemical Engineering

formerly

CANADIAN JOURNAL OF TECHNOLOGY

CONTENTS

Turbulent Heat and Mass Transfer from Stationary Particles	*I. S. Pasternak* *W. H. Gauvin*	35
The Effect of Temperature on the Fluidization of Silver Powders	*E. Echigoya* *G. L. Osberg*	43
Letter to the Editor—Erratum	*G. W. Hodgson* *M. E. Charles*	45
A Method for the Determination of Tie-Lines in Ternary Liquid Systems	*E. L. Heric* *Ronald M. Rutledge*	46
Machine Computations for Transient Stagewise Processes	*D. Yesberg* *A. I. Johnson*	49
Preparation of Aluminum Octanoate and Aluminum Isooctanoate	*J. A. Wheat* *D. A. MacLeod* *R. G. Dunlop* *H. Sheffer*	55
The Upward Vertcial Flow of Air-Water Mixtures. III. Effect of Gas Phase Density on Flow Pattern, Holdup and Pressure Drop	*R. A. S. Brown* *G. A. Sullivan* *G. W. Govier*	62

Published by
THE CHEMICAL INSTITUTE OF CANADA
OTTAWA CANADA

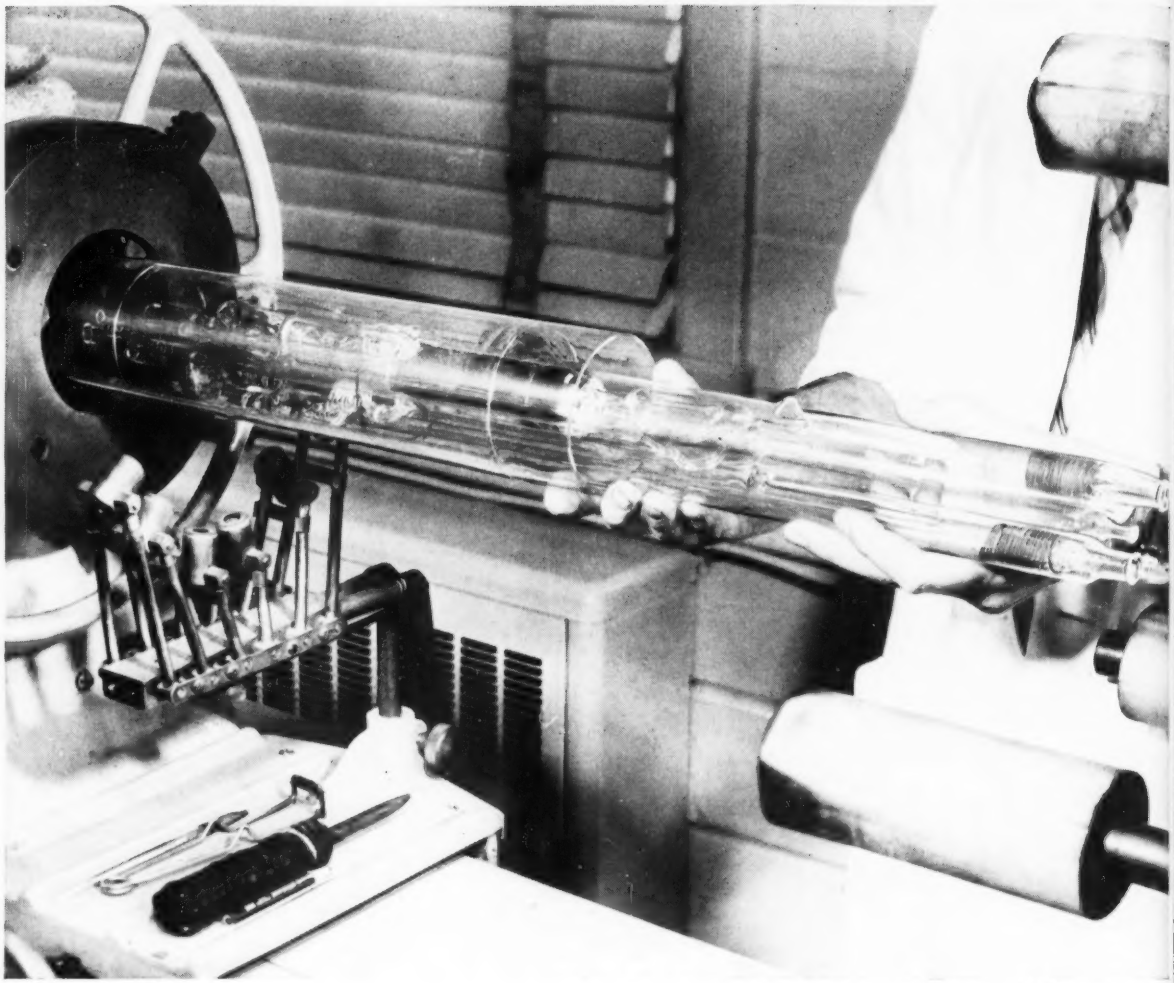

Photograph taken at C-I-L Central Research Laboratory, McMasterville, Que.

POLYMERIC PRECISION

This is an ebulliometer—being assembled by the master glass-blower on his own lathe at our Central Research Laboratory.

The ebulliometer uses two vapor lift pumps such as those found in electric coffee percolators. One circulates a polymer solution while the other circulates boiling solvent—each liquid stream is directed over a temperature detector so sensitive that a difference of one-millionth of 1°C. may be sensed. This device allows the measurement of high molecular weights related to the physical properties of polymers.

Such C-I-L research contributes to higher standards of performance in the plastics industry . . . to new and better plastic products . . . and—through better technical service—to greater success in the application of these new materials to modern living.

C-I-L

CANADIAN INDUSTRIES LIMITED

Serving Canadians Through Chemistry

Agricultural Chemicals • Ammunition • Coated Fabrics • Industrial Chemicals • Commercial Explosives • Paints • Plastics • Textile Fibres

The Canadian Journal of Chemical Engineering

formerly

Canadian Journal of Technology

VOLUME 38 APRIL, 1960 NUMBER 2

Editor
A. Cholette
Faculty of Science, Laval University
Quebec, Que.

Managing Editor
T. H. G. Michael

Publishing Editor
D. W. Emmerson

Assistant Publishing Editors
R. G. Watson
R. N. Callaghan

Circulation Manager
M. M. Lockey

EDITORIAL BOARD

Chairman
W. M. CAMPBELL, Atomic Energy of Canada Limited,
Chalk River, Ont.

L. D. DOUGAN, Polymer Corp. Limited,
Sarnia, Ont.

W. H. GAUVIN, McGill University,
Montreal, Que.

G. W. GOVIER, University of Alberta,
Edmonton, Alta.

J. W. HODGINS, McMaster University,
Hamilton, Ont.

A. I. JOHNSON, University of Toronto,
Toronto, Ont.

E. B. LUSBY, Imperial Oil Limited,
Toronto, Ont.

LEO MARION, National Research Council,
Ottawa, Ont.

R. R. McLAUGHLIN, University of Toronto,
Toronto, Ont.

G. L. OSBERG, National Research Council,
Ottawa, Ont.

J. H. SHIPLEY, Canadian Industries Limited,
Montreal, Que.

H. R. L. STREIGHT, Du Pont of Canada Limited,
Montreal, Que.

EX-OFFICIO

E. GORDON YOUNG, President, The Chemical Institute of Canada.

H. BORDEN MARSHALL, Chairman of the Board of Directors.

H. S. SUTHERLAND, Director of Publications.

Authorized as second class mail, Post Office Department, Ottawa. Printed in Canada

Manuscripts for publication should be submitted to the Editor: Dr. A. Cholette, Faculty of Science, Laval University, Boulevard de l'Entente, Quebec, Que. (Instructions to authors are on the next page).

Editorial, Production and Circulation Offices: 48 Rideau Street, Ottawa 2, Ont.

Advertising Office: C. N. McCuaig, manager of advertising sales, *The Canadian Journal of Chemical Engineering*, Room 601, 217 Bay Street, Toronto, Ont. Telephone—EMpire 3-3871.

Plates and Advertising Copy: Send to *The Canadian Journal of Chemical Engineering*, 48 Rideau Street, Ottawa 2, Ont.

Subscription Rates: In Canada—$3.00 per year and 75c per single copy; U.S. and U.K.—$4.00; Foreign—$4.50.

Change of Address: Advise Circulation Department in advance of change of address, providing old as well as new address. Enclose address label if possible.

The Canadian Journal of Chemical Engineering is published by The Chemical Institute of Canada every two months.

Unless it is specifically stated to the contrary, the Institute assumes no responsibility for the statements and opinions expressed in *The Canadian Journal of Chemical Engineering*. Views expressed in the editorials do not necessarily represent the official position of the Institute.

The Canadian Journal of Chemical Engineering

INSTRUCTIONS TO AUTHORS

Manuscript Requirements for Articles

1. The manuscript should be in English or French.
2. The original and two copies of the manuscript should be supplied. These are to be on 8½ x 11 inch sheets, typewritten, and double spaced. Each page should be numbered.
3. Symbols should conform to American Standards Association. An abridged set of acceptable symbols is found in the third edition of Perry's Chemical Engineers' Handbook. Greek letters and subscripts and superscripts should be carefully made.
4. Abstracts of not more than 200 words in English indicating the scope of the work and the principal findings should accompany all technical papers.
5. References should be listed in the order in which they occur in the paper, after the text, using the form shown here: "Othmer, D. F., Jacobs, Jr., J. J., and Levy, J. F., Ind. Eng. Chem. **34**, 286 (1942). Abbreviations of journal names should conform to the "List of Periodicals Abstracted by Chemical Abstracts". Abbreviations of the common journals are to be found in Perry's Handbook also. All references should be carefully checked with the original article.
6. Tables should be numbered in Arabic numerals. They should have brief descriptive titles and should be appended to the paper. Column headings should be brief. Tables should contain a minimum of descriptive material.
7. All figures should be numbered from 1 up, in Arabic numerals. Drawings should be carefully made with India ink on white drawing paper or tracing linen. All lines should be of sufficient thickness to reproduce well, especially if the figure is to be reduced. Letters and numerals should be carefully and neatly made, with a stencil. Generally speaking, originals should not be more than twice the size of the desired reproduction; final engravings being 3¼ in. or 7 in. wide depending on whether one column or two is used.
8. Photographs should be made on glossy paper with strong contrasts. Photographs or groups of photographs should not be larger than three times the size of the desired reproduction.
9. All tables and figures should be referred to in the text.

Submission of Manuscripts

1. The three copies of the manuscript, including figures and tables, should be sent directly to:
   DR. A. CHOLETTE, editor,
   The Canadian Journal of Chemical Engineering,
   Faculty of Science, Laval University,
   Boulevard de l'Entente,
   Quebec, Que.
2. The authors addresses and titles should be submitted with the manuscript.
3. The author may suggest names of reviewers for his article, but the selection of the reviewers will be the responsibility of the editor. Each paper or article is to be reviewed by two chemical engineers familiar with the topic. Reviewers will remain anonymous.
4. All correspondence regarding reviews should be directed to the editor.

Reprints

1. At least 50 free "tear sheets" of each paper will be supplied.
2. Additional reprints may be purchased at cost. An estimated cost of reprints, with an attached order form, will be sent to the author with the galley proofs.
3. Orders for reprints must be made before the paper has appeared in the Journal.

Communications, Letters and Notes to the Editor

Short papers, as described below, will be considered for publication in this Journal. Their total length should not exceed 600 words, or its equivalent.

Communications

A communication is a prompt preliminary report of observations made which are judged to be sufficiently important to warrant expedited publication. It usually calls for a more expanded paper in which the original matter is republished with more details.

Letters

A letter consists of comments or remarks submitted by readers or authors in connection with previously published material. It may deal with various forms of discussion arising out of a publication or it may simply report and correct inadvertent errors.

Notes

A note is a short paper which describes a piece of work not sufficiently important or complete to make it worth a full article. It may refer to a study or piece of research which, while it is not finished and may not be finished, offers interesting aspects or facts. As in the case of an article a note is a final publication.

* * *

Turbulent Heat and Mass Transfer from Stationary Particles[1]

I. S. PASTERNAK[2] *and W. H. GAUVIN*[3]

Convective heat and mass transfer rates for 20 shapes suspended in various orientations in a hot turbulent air stream were correlated by the equation:

$$j'_D = 0.692\ (Re'')^{-0.486} \text{ for } 500 < Re'' < 5000$$

for turbulent intensities between 9 and 10%, using a new characteristic dimension, L'', in the Reynolds Number. This dimension, defined as the total surface area divided by the maximum perimeter perpendicular to flow, was qualitatively explained from boundary layer considerations and was found to correlate the data for different shapes available in the literature. Qualitative pictures for the relative rates of heat and mass transfer around the various shapes were also obtained.

A large amount of experimental evidence has been reported in the literature on heat and mass transfer coefficients for standard bodies such as cylinders, spheres and flat plates, but little information is available on other shapes such as disks, prisms, rings, granular particles or fibres. Since the latter are finding increasing use in practical engineering applications, such as flash drying and many solids-gas contacting operations, modifications to existing correlations are required to account for the influence of the shape on the transfer phenomena. A more fundamental approach to the problem would be to define a uniform particle characteristic dimension by means of which all data on heat and mass transfer could be correlated, irrespective of the shape of the particle.

A survey of the published literature shows that many "particle diameters" have been proposed by various authors in an attempt to define a particle of non-standard shape[1, 2, 3, 4]. The most commonly used diameter for a single particle (and the easiest to determine) appears to be the equivalent diameter, d_p, the diameter of a sphere of equal volume, while d_s, the diameter of a sphere of equivalent surface area, has also been used. In the field of multiparticle technology, such as in the flow of fluids through packed beds, Wadell's sphericity ψ[5], Carman's $\phi_c\ (= \psi)$[6] as well as Leva's $\lambda\ (= 1/\psi)$[7] have become popular as a means of designating the average shape of a particle. However, these particle diameters and shape factors all suffer from a common disadvantage — they constitute a fixed property of a particular shape without reference to the particle orientation.

[1]*Manuscript received October 29, 1959; Accepted January 11, 1960.*
[2]*Imperial Oil Limited, Sarnia, Ont.*
[3]*McGill University and Pulp and Paper Research Institute of Canada, Montreal, Que.*

In 1940, Powell[8] showed that both particle shape and orientation had a large effect on the rate of heat and mass transfer, but he made no attempt to correlate either of these factors into the existing transfer equations i.e. the Nusselt equation[9, 10, 11] and the Chilton-Colburn equation [12, 13, 14, 15]. The validity of these equations is now well established and they are commonly used to correlate the individual heat and mass transfer data for single spheres, cylinders and flat plates, provided that the diameter, for both the sphere and the cylinder, or the length of the flat plate in the flow direction, is used as the characteristic dimension in the Reynolds Number (and in the Nusselt Number if it is employed).

In 1953, Krischer[16] suggested the use of a characteristic length which would take into account both the shape and orientation of a particle and defined a "flow length", L_K, as the length of the path covered by the streaming medium along the transfer surface. Using this flow length in the Nusselt equation, he was partially successful in recorrelating some of the data reported for the three standard shapes[17]. In an attempt to improve this correlation, Krischer and Loos[9, 10] investigated the effect of fourteen shapes on the rate of heat and mass transfer. The results of their work will be discussed in more detail later; it should be noted at this time, however, that — because of the high value of the length-to-diameter ratio of the shapes they investigated — their characteristic length, L', may be considered as useful for two-dimensional shapes only.

In the present investigation three-dimensional shapes were studied with the following objectives: (1) To obtain convective heat and mass transfer data for stationary spheres and to compare the results with those in the literature; and (2) To determine and compare convective heat and mass transfer data for other shapes in various orientations in a fluid stream in order to define a new characteristic dimension which will depend not only on the particle shape but on its orientation as well.

EXPERIMENTAL

The rates of heat and mass transfer during the evaporation of water from different stationary particles were studied in a 1 1/2-in. diameter pyrex glass column in which turbulent air was passed under controlled conditions of temperature, humidity and velocity.

Particle Shapes

After much investigation, Celite was selected as the material from which the particles were made, because of its strength, inertness, and workability. The dimensions of the particles remained completely unaffected by moisture or air temper-

ature. Since Celite is composed of a microporous structure of minute silica particles — approximately four microns in size — held together by a bentonite clay binder, it loses most of its moisture at constant rate. An important added feature is that Celite changes color from orange to a pale yellow on drying, allowing a qualitative picture of the rate of mass transfer around a particular shape to be obtained.

The various shapes investigated in this study, their dimensions and orientation in the flow stream, are given in Table 1.

Apparatus

Figure 1 shows a schematic diagram of the apparatus. It consisted essentially of two 1½-in. i.d., 12-in. long Pyrex glass columns in parallel, through which hot air could be passed, installed in a large electrically-heated, constant-temperature oil bath equipped with heaters, a cooling coil and a stirrer. The hot air from the ¼-in. supply line entered the bottom of one of the columns and passed in succession through a 1-in. diameter orifice and a 14-mesh wire screen, 2½ inches apart. A flat

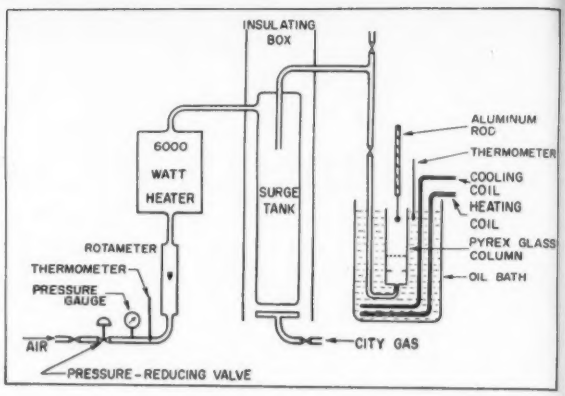

Figure 1—Schematic diagram of apparatus for stationary shapes.

TABLE 1

PARTICLE SHAPES AND DIMENSIONS

Shape and Orientation	Particle Designation and Dimensions	Results
	Spheres	*S*1: d = 0.458 in. *S*2: d = 0.365 in. *S*3: d = 0.290 in. *S*4: d = 0.220 in.	Figure 4
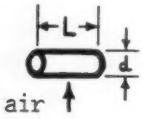	Cylinders (Disk)	*C*1: d = 0.380 in.; L = 0.405 in. *C*2: d = 0.197 in.; L = 0.405 in. *C*3: d = 0.378 in.; L = 0.157 in.	Figure 5(A)
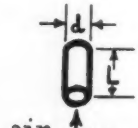	Cylinders	*C*4: d = 0.264 in.; L = 0.412 in. *C*5: d = 0.266 in.; L = 0.229 in. *C*6: d = 0.264 in.; L = 0.158 in. *C*7: d = 0.481 in.; L = 0.410 in.	Figure 5(B)
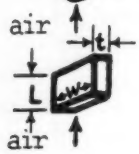	Prism	*P*1: w = 0.379 in.; L = 0.377 in. t = 0.150 in.	Figure 6(A)
	Cubes	*P*2: L = 0.360 in. *P*3 L = 0.252 in.	Figure 6(A)
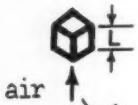	Cubes	*P*4: L = 0.282 in. *P*5: L = 0.244 in.	Figure 6(B)
	Cube	*P*6: L = 0.284 in.	Figure 6(B)
	Hemispheres	*H*1: d = 0.494 in.; L = 0.247 in. *H*2: d = 0.503 in.; L = 0.251 in. *H*3: d = 0.497 in.; L = 0.222 in. *H*1a: d = 0.494 in.; L = 0.247 in.	Figure 7

velocity profile was thus obtained two inches from the top of the column, where each of the particles was suspended.

A particle under test was suspended in place at the end of a 3-in. long hypodermic needle held rigidly at the end of a small powerful permanent magnet embedded into the end of a long aluminum rod. In this way the particle remained free from vibrations in the air stream, and yet could be removed at will for weighing.

The air was supplied by a large compressor, and passed in succession through a pressure-reducing valve, a calibrated rotameter, a 6000-watt electrical heater and finally into a large heated surge tank from which it was led to the Pyrex columns through the insulated ¾-in. supply line. Its temperature was maintained at a preset value by an indicating temperature controller which regulated the electrical input to the heaters. In any one experimental run, the temperature of the air passing through the Pyrex column and the temperature of the oil bath were held at the same value to eliminate the occurrence of natural convection currents which would have been caused by cooler column walls.

Procedure

After completely steady conditions of air velocity and temperature had been attained in the apparatus, a Celite particle of known shape, weight and moisture content was suspended in a definite orientation in the glass column. As drying proceeded, the particle was weighed every few minutes by means of a delicate quartz-spiral balance, the extension of which was measured through a telescope. Each run was continued until the orange (wet) Celite turned a pale yellow color, indicating that the drying had passed from the constant-rate into the falling-rate period. The wet- and dry-bulb temperatures of the air in the column were accurately measured before and after each run so that the wet-bulb temperature of the particle as well as the air humidity could be recorded.

Turbulence Intensity of Air Stream

The velocity and turbulence intensity profiles for air passing through the empty column were obtained by means of a Model HWB2 Flow Corporation hot wire anemometer equipped with a HWP-B tungsten wire (0.00035-in. diameter) probe. The results obtained at two air velocities are shown in Table 2. The determinations were made at a cross-section 2¾-in. below the top of the 12-in. long column and ¾-in. below the position where a particle was normally suspended in the column. The flatness of the velocity profile should be noted.

TABLE 2

AIR VELOCITY AND TURBULENCE INTENSITY PROFILES

Fraction of column diameter	Air velocity ft./sec.	Intensity of turbulence %	Air velocity ft./sec.	Intensity of turbulence %
0.25	22.1	9.1	10.6	10.3
0.50	23.1	9.2	10.8	10.0
0.75	22.4	–	11.6	–

Treatment of Experimental Data

The results from each experimental run were processed so that they could be used in the form of a modified Chilton-Colburn equation[12]:

$$j'_D = \frac{k_G P_{LM}}{G_m} (Sc)^{2/3} = a(Re'')^{-b} \quad \ldots\ldots\ldots\ldots (1)$$

where a and b are constants, and Re'' is the particle Reynolds Number, based on its characteristic dimension.

The reason for this choice of correlation was twofold: (*a*) it may be seen by rearranging the variables, that a plot of the modified Nusselt Number for mass transfer, Nu', as a function of Re'' is in reality a plot of $(j'_D)\ (Re'')\ (Sc)^{1/3}$ against Re'', so that it is more direct to plot j'_D against Re'' immediately and (*b*) the characteristic dimension, or diameter d, appears on both sides of the Nusselt equation while it appears only in the Reynolds Number in the Chilton-Colburn expression. This makes the data for the latter equation easier to rearrange and plot, especially in view of the fact that the object of this investigation was to find the value of the characteristic dimension.

In determining Re'', values of viscosity and density were used at the average temperature of the gas film around the particle. Average values for the air velocity across the column were also used. For j'_D, the mass transfer coefficient k_G was calculated from the loss in water per unit time, the mass of the particle as well as the driving force involved between the vapor pressure of the water at the wet-bulb temperature at the surface of the particle and the partial pressure of water in the air stream. The Schmidt Number, Sc, was verified to be constant over the range of temperatures used; the diffusivity data for water evaporating in air being obtained from the International Critical Tables[18].

Experimental Results

One hundred and sixteen runs were carried out on the 20 shapes described in Table 1 over the following range of operating conditions: air velocities, from 4 to 25 ft./sec.; air temperatures, from 70° to 250°F.; air humidities, from 0.003 to 0.010 lb. water/lb. dry air.

Figure 2 shows the qualitative observations obtained from changes in color of the Celite during the drying process of the various shapes. On this diagram the distance between the shape outline and the corresponding envelope at a particular point gives a measure of the relative rate of heat and mass transfer at that point. Shaded parts show areas of minimum transfer.

Figure 3 shows the calculated results plotted (with the exception of those for cylinders with their lengths parallel to the air stream) in the form of Equation (1) — with a possible error of ± 15% — using a new particle characteristic dimension, L'', instead of the usual diameter, d, in the Reynolds Number. This new characteristic dimension, L'', for a stationary particle of any shape suspended in a moving fluid stream in a definite orientation is defined as the total surface area of the particle divided by the perimeter of the maximum projected area perpendicular to flow. As an example, for a cylinder of length, L, and diameter, d, suspended with its length perpendicular to flow:

$$L'' = \frac{\text{surface area}}{\text{max. perimeter}} = \frac{\pi dL + 2\pi d^2/4}{2\,(L + d)} \quad \ldots\ldots\ldots (2)$$

When the cylinder has a high aspect ratio, i.e., when L is much greater than d:

$$L'' = \frac{\pi d}{2} = L'$$

where L' is the characteristic "flow length" as defined by Krischer and Loos.

Discussion of Results

Spheres

Figure 4 shows the results for four spheres plotted and correlated by the following generalized equation with an average deviation of ± 10% (for a sphere, $L'' = d$ and $Re'' = Re$):

$$j'_D = 0.692\ (Re'')^{-0.488} \quad \ldots\ldots\ldots\ldots\ldots (3)$$

Since no special trend in the scatter of points can be noted for each of the comparatively large spheres used, the wall effect on the rate of heat and mass transfer was considered to be negligible or constant — within the experimental deviation. Because the size range for all other shapes was similar to that of

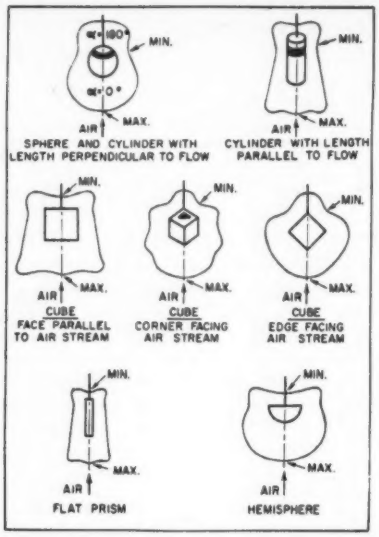

Figure 2 — Qualitative transfer rates around the shapes used.

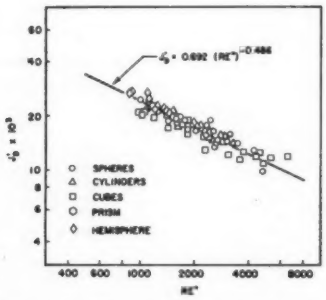

Figure 3—Results for shapes used.

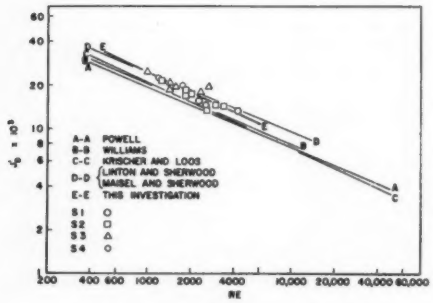

Figure 4—Data for spheres.

spheres, the wall effect was neglected throughout the investigation.

Figure 4 also shows the data of Powell[8], Williams[19], Maisel and Sherwood[14], Linton and Sherwood[13] and Krischer and Loos[9, 10]. It may be seen that the proposed correlation differs slightly in slope from the experimental lines of the other investigators but falls between them. The scatter in the data from the other investigators may be partly due to the fact that in some cases the average velocity across the column was used — as in this investigation — while in other cases only the approach velocity to the particle was measured; it may also be partly due to the fact that each investigation was carried out under different conditions of fluid turbulence. Only recently have attempts been made to correlate the turbulence parameters with heat and mass transfer rates[15, 20, 21, 22].

Qualitatively it was observed that the maximum rate of heat and mass transfer occurred over the front half of the sphere with a second maximum occurring at the rear — around the point of suspension. A wet ring around the sphere at from 100 to 110° from the stagnation point indicated the position of minimum transfer. These observations agree with those of Cary[23] as well as those of Garner[24] who noted that for a solid sphere at Reynolds Numbers greater than 500 the minimum mass transfer rate occurred at approximately 105° from the stagnation point.

Cylinders

(a) Length perpendicular to flow. Figure 5 (*A*) shows that not only have cylinders of different length-to-diameter ratios been correlated with spheres, but a disk (*C*3) also appears to follow the same behavior.

The heat and mass transfer flux around a cylinder in this orientation, as shown in Figure 2, agreed well with the observations of Robinson and Han[25] and Winding and Cheney[26] who noted a maximum Nusselt Number at the front and rear of the cylinder with a minimum at approximately 90° from the stagnation point. The rate of heat and mass transfer from the two flat sides of the cylinder was intermediate between the minimum and maximum values.

(b) Length parallel to flow. Figure 5(*B*) shows that the correlation line does not follow the line for spheres completely but breaks away at $Re'' = 1000$, presumably because at higher values the boundary layer becomes turbulent. This explanation is based on a possible analogy with the plot given in the Chemical Engineers' Handbook[27] for the rate of heat and mass transfer from plane and cylindrical surfaces located parallel to the direction of flow. This plot compared the data of Pasquill[28], Wade[29] and Powell[8] with the theoretical equations of Pohlhausen[30] and Latzko[31], and clearly establishes the regions where the laminar and turbulent transfer rates occur. In this investigation, early transition to a turbulent boundary layer may well be caused by the sharp edge around the upstream diameter.

It was observed that for a cylinder in this orientation the position of the minimum transfer point, which occurred on a circular band around the rear portion (see Figure 2), did vary with air velocity. However, no definite conclusions could be drawn regarding its changes in location with increasing Reynolds Numbers. An increase in the relative heat and mass transfer rate around the edges is probably due to a thinning of the boundary layer in these regions.

Prism

Only six experimental points were obtained for a flat prism suspended with its faces parallel to the air stream and the results shown in Figure 6(*A*) are inconclusive. It cannot be ascertained whether the single point below the sphere correlation is due to an experimental error while the first five points indicate a tendency for a turbulent boundary layer to be formed, or whether all the points just show an experimental scatter of $\pm 16\%$ about the sphere line. The latter case is also possible since it was extremely difficult to suspend a prism with its faces exactly parallel to the air stream. Qualitatively the maximum transfer rates occurred at the front with the minimum at the rear, as shown in Figure 2. Again high transfer around the edges was noted.

Cubes

(a) Face parallel to air stream. In this case Figure 6(*A*) shows that all results follow the correlation for spheres quite faithfully in the range of Reynolds Numbers and for the two cube sizes investigated.

(b) *Corner facing the air stream.* The results in this case follow the line for spheres but are somewhat lower, as shown in Figure 6(*B*). The reason could well reside in the suspension method, as any departure from the exact position would cause a decrease in the actual value of the perimeter, thus making the value of L'' larger than that calculated.

(c) *Edge facing the air stream.* Figure 6(*B*) shows that the results are entirely similar to the previous ones, quite possibly for the same reason.

For the cube in case (a) : $L'' = 1.50\ L$
For the cube in case (b) : $L'' = 1.41\ L$
For the cube in case (c) : $L'' = 1.25\ L$

where L is the length of one side of the cube.

The transfer fluxes for the cubes in the three orientations were observed to be approximately as shown in Figure 2. For all three cubes the rate of heat and mass transfer around the edges appeared to be very high relative to the other areas. The minimum point of transfer is noted by the shaded area.

Hemisphere

Figure 7 clearly establishes the validity of using L'' for hemispheres (*H*1 and *H*2), or part of a hemisphere (*H*3). However, for hemisphere *H*1*a*, in which the flat rear section was covered with an impervious layer of Pliabond cement, the data fall about 40-50% higher than the sphere line. This behavior was to be expected in view of the fact that previous published results for a sphere have shown that the ratio of the mass transfer before the point of separation to that after the point of separation is of the order of 75 to 25, depending on the magnitude of the Reynolds Number[24]. From Figure 7 it may be shown that the ratio of mass transfer on the curved surface of the hemisphere (before the point of separation) to that on the flat surface (after the point of separation) is 96.5 to 3.5 at $Re'' = 1000$ and 87.1 to 12.9 at $Re'' = 3000$. These ratios are of course independent of the characteristic dimension used for the particle diameter.

Correlation of Data in Literature Using L"

Further confirmation for the validity of Equation (3) was sought from the published literature. A search revealed few investigations where more than one shape had been used. The six major ones which were thus found were correlated and replotted in the form of $j'_D - Re''$ graphs. These graphs are shown in Figures 8 to 11 inclusive.

Data of Maisel and Sherwood[14]

Maisel and Sherwood reported their results for spheres, cylinders (axis perpendicular to air flow) and disks (diameter perpendicular to air flow) in the form of three separate $j'_D - Re$ graphs. Since they were mainly interested in obtaining accurate evaporation data for various volatile liquids, no attempt was made to present a unified correlation. Figure 8(*A*) shows their data correlated with that of a sphere using L'' as the characteristic dimension. It may be seen that the agreement is excellent and that a single correlation could replace their three plots quite effectively.

Data of Linton and Sherwood[13]

Linton and Sherwood also reported their results for spheres, cylinders and flat plates in the form of separate $j'_D - Re$ graphs. Figure 8(*B*) shows their results for the benzoic acid sphere and cylinder and the cinnamic acid flat plates correlated by the use of L''. The change in slope for the flat plates, indicating the formation of a turbulent boundary layer, should be noted.

Data of Norris and Spofford[32]

These authors presented in 1942 a generalized correlation for convective heat transfer from pin fins and strip fins of various

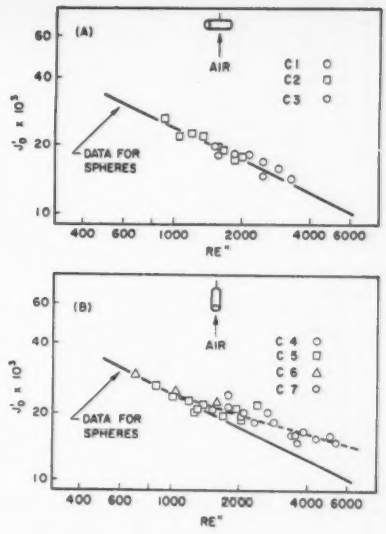

Figure 5—Data for cylinders.

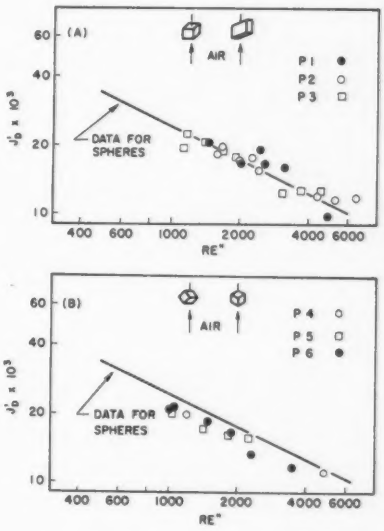

Figure 6—Data for prism and cubes.

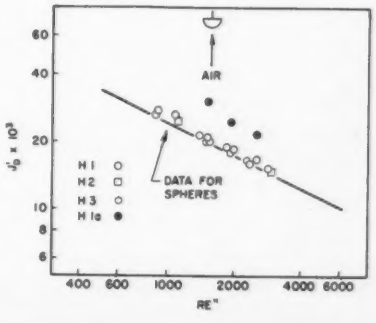

Figure 7—Data for hemispheres.

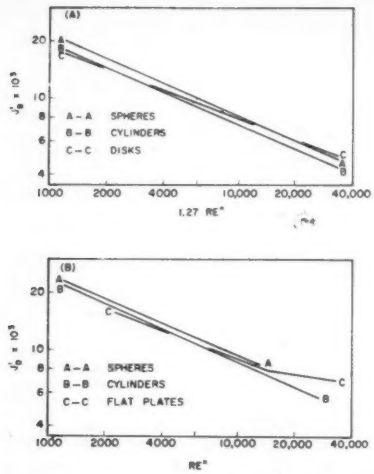

Figure 8(A)—Data of Maisel and Sherwood.
Figure 8(B)—Data of Linton and Sherwood.

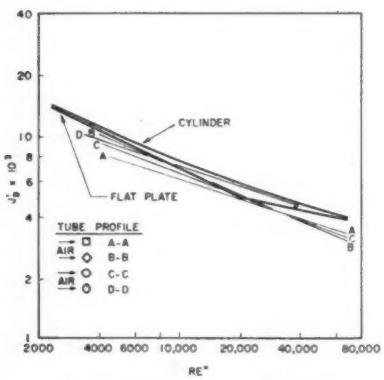

Figure 10—Data of Hilpert.

designs, and compared their results with the data of Fage and Falkner[33] for a single plane, the data of Colburn[34] for a single cylinder with its length perpendicular to the air flow, and the data of Grimison[35] for a bank of cylinders. They presented their correlation and comparison data in the form of a $j_H - Re_p$ graph and obtained the equation:

$$j_H = (Re_p)^{-0.50} \quad \ldots\ldots\ldots\ldots\ldots\ldots\ldots\ldots (4)$$

where j_H—heat transfer factor;

Re_p—Reynolds Number based on the perimeter, P, of the shapes.

It may be shown that for all the shapes used and correlated, the authors were using $P = 2L''$ (approximately) as their shape parameter. Figure 9 shows their graph replotted using L'' in the Reynolds Number. The agreement in correlation and comparison is good.

Data of Hilpert[36]

Figure 10 shows Hilpert's data for a long cylinder and long tubes of various profiles, replotted in terms of L'' and compared with Colburn's equation for a flat plate. Again the correlation appears to be good. This graph indicates the variations that may be expected when dealing with bodies of different shape.

Data of Powell[8]

Figure 11 shows Powell's data replotted and correlated by means of L'', assuming an air temperature of 20°C. The heat and mass transfer coefficients for the circular disks and rectangular plates facing the air stream (lines *E-E* and *G-G*) were

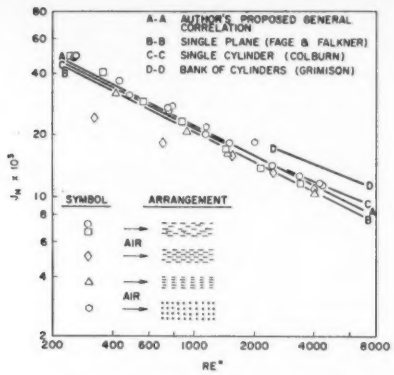

Figure 9—Data of Norris and Spofford.

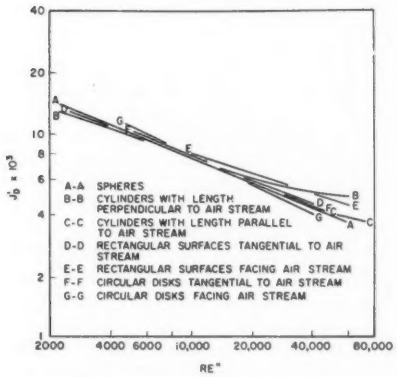
A-A SPHERES
B-B CYLINDERS WITH LENGTH PERPENDICULAR TO AIR STREAM
C-C CYLINDERS WITH LENGTH PARALLEL TO AIR STREAM
D-D RECTANGULAR SURFACES TANGENTIAL TO AIR STREAM
E-E RECTANGULAR SURFACES FACING AIR STREAM
F-F CIRCULAR DISKS TANGENTIAL TO AIR STREAM
G-G CIRCULAR DISKS FACING AIR STREAM
RE*

Figure 11—Data of Powell.

obtained with water evaporating from the front surface only. However, in calculating L'' for these shapes, the total surface area of both sides of the thin shapes was used rather than just the "wetted" area. The resulting correlation shows that the type of flow around a particle is dependent only on the particle dimensions (as it should be) and is independent of the area active for heat and mass transfer. When the wetted areas faced downstream, the heat and mass transfer rates were from 10-40% lower.

Data of Krischer and Loos[9,10]

In 1958 Krischer and Loos obtained a definition for the characteristic length, L', of an irregular particle by studying the rate of heat and mass transfer from 14 shapes. All these shapes were long and thin, i.e., they had a high aspect ratio. On the basis of this rather restricted particle geometry, they defined L' as the length of one side of a rectangle whose surface area is equal to one half the surface area of the body and whose other side has a length equal to the length of the shape perpendicular to the direction of flow. For a shape whose surfaces were only partially involved in the transfer processes, the average L' was taken as half the length of the development of the exchange area.

It should be noted that for all the shapes used by Krischer and Loos except spheres, L'' is approximately equal to L'. However, L'' for a particular shape appears to be less arbitrary, easier to define and more practical to use. More important still, L' does not apply to a particle shape whose dimensions along all three axes are roughly similar. Thus for a sphere $L' = \pi d/2$, while $L'' = d$.

Krischer and Loos' following general conclusions are worthy of note: (a) L' can be used as the characteristic length for any given shape (with a high aspect ratio) with sufficient exactness to correlate the heat and mass transfer coefficients with the

Reynolds Number (± 15 percent) provided that no recessed surfaces are present. (b) For bodies with recessed surfaces, low heat and mass transfer results are obtained at low Reynolds Numbers (<2500) but approach the values for standard shapes (spheres, cylinders and flat plates) at high Reynolds Numbers (>2500). The low values are due to dead areas of fluid with little turbulence in the cavities. (c) For a body whose true surface and flow length L' are difficult to define, the "sheath area" and its flow length are better relative values to use than the surface area and flow length of a sphere or a cylinder of the same volume. (d) For all bodies with recessed surfaces, the sheath area appears to be the most suitable value for small Reynolds Numbers whereas for large Reynolds Numbers, the true surface area appears to be the better relative value for the determination of heat and mass transfer.

Fundamental Significance of L''

The present stage of development of the Boundary Layer Theory does not allow the derivation of a mathematical expression to show why L'' should account for the three-dimensional effects of particle shape and orientation. It does, however, enable a qualitative understanding of its meaning to be obtained.

From the general properties of a laminar boundary layer, it is known that the *local* heat transfer coefficient h in the equation:

$$dq = h\,dA\,(T_b - T_s) \qquad (5)$$

is inversely proportional to the thickness, δ_T, of the thermal boundary layer, which is itself related to the thickness, δ_v, of the velocity boundary layer and is nearly equal to it for a Prandtl Number of one. In addition, it is known that the Nusselt Number is proportional to $(Re)^{1/2}$ and hence h (or k_G) is inversely proportional to the square root of the characteristic dimension used to define the Reynolds Number. However, to integrate Equation (5) for any body up to the point of separation (assuming constant temperatures):

$$q = K_1\,(T_b - T_s)\int \frac{dA}{\delta_T} \qquad (6)$$

the manner in which δ_T varies as integration along the surface proceeds must also be known. This can be calculated for flat plates, regular and elliptical cylinders, spheres and a few other shapes[37], but the calculations become hopelessly complex for the shapes used in this investigation due to such factors as the possible separation and later re-attachment of the boundary layer at sharp forward edges.

Since for a sphere δ_T is anywhere proportional to $d^{1/2}$ for a laminar boundary layer up to the point of separation (and proportional to $d^{0.20}$ for a turbulent boundary layer) it is natural to take the diameter d of the sphere as its basic characteristic dimension for use in heat (and mass) transfer correlations. Once these correlations have been established for spherical particles (as was done in this investigation) it is logical to apply them in their original form to other shapes by using the proper characteristic dimension. The problem thus resolves itself in finding, for any shape in any orientation, a characteristic dimension which — in an *overall* or *integrated* way (as distinct from local) — will account for the average thickness of the boundary layer.

It can be verified — from the limited evidence available — that L'' as defined appears to fulfill this requirement from both perimeter and surface area considerations. Thus, for shapes with a constant maximum perimeter, L'' for any shape will increase as the surface area is increased, from its definition. But as the latter is increased, the boundary layer will thicken[37], Figure 7.7) to cause an overall decrease in the integrated value of h (or k_G). This is in agreement with the theory just presented that h is inversely proportional to the square root of a characteristic dimension. From Equation (3) — obtained experimentally —it is evident that:

$$k_G\,(\text{overall}) \propto 1/(L'')^{0.486}$$

For shapes with a constant surface area, L'' for any shape will increase as the perimeter is decreased, from its definition. However, when the latter is decreased, the boundary layer also thickens[37], Figure 12.11) and an overall decrease in the integrated value of h (or k_G) will result. Again agreement of experimental values with theory is obtained when L'' is used as the characteristic dimension.

CONCLUSIONS

1. A new dimension, L'', characteristic for single, stationary particles in a fluid stream, was introduced to account for both particle shape and orientation in the forced convection heat and mass transfer equations. This dimension is defined as the total surface area of the particle divided by the perimeter of the maximum projected area perpendicular to flow.

2. The heat and mass transfer data for 20 shapes in different orientations were correlated with the aid of L'' by the equations:

$$j'_D = 0.692\,(Re'')^{-0.486} \text{ for } 500 < Re'' < 5000$$

with a deviation of ± 15%. This equation can be readily expressed in terms of the Nusselt Number for mass transfer, Nu', since $Nu' = j'_D\,(Re'')\,(Sc)^{1/3}$, yielding the form: $Nu' = 0.692\,(Re'')^{0.514}\,(Sc)^{1/3}$. It can similarly be expressed in terms of the Nusselt Number, Nu.

3. The results for spheres were correlated by this equation with a deviation of ± 10%, and agreed quite well with published data.

4. All the heat and mass transfer data in this investigation were obtained at an intensity of turbulence between 9 and 10%.

5. Qualitative pictures for the relative rates of heat and mass transfer around the various shapes used were presented (Figure 2).

6. L'' appears to be a more general shape parameter than Krischer and Loos' L'. It was found to correlate the various data for shapes available in the literature — including those of Krischer and Loos.

7. The general conclusions of Krischer and Loos concerning shapes with recessed surfaces or surfaces which are difficult to define probably apply when using L'' instead of L'. but this assumption still requires experimental confirmation.

8. A qualitative explanation for the meaning of L'' was presented from boundary layer theory considerations. These considerations show that the use of L'' as a characteristic dimension does account for the thickness of the boundary layer around a specific particle.

Acknowledgements

Financial assistance from Canadian Refractories Limited in the form of two fellowships to one of the authors, I. S. Pasternak, and from the National Research Council in the form of a research grant, is gratefully acknowledged. Recognition is also due to the Pulp and Paper Research Institute of Canada for the loan of equipment and for the extensive use of workshop and library facilities.

Nomenclature

Roman Signals

a and b = constants in Equation (1).
A = surface area of particle, ft.²
A_p = surface area of a sphere with same volume as particle, ft.²
c_p = specific heat of air at constant pressure, B.t.u./(lb.)(°F.).
d = diameter, ft.; (d_p, equivalent diameter).
d' = diameter of flat (back) part of hemisphere, ft.
D_v = diffusion coefficient for water evaporating in air, ft.²/hr.
G = mass velocity of flowing air, lb./(ft.²)(hr.).
G_m = molal mass velocity of flowing air, lb. moles/(ft.²)(hr.).
h = heat transfer coefficient, B.t.u./(hr.)(ft.²)(°F.).
k_f = average thermal conductivity of air film, B.t.u./(hr.)(ft.)(°F.).
k_G = mass transfer coefficient, lb. moles/(hr.)(ft.²)(Δp).
K_1 = constant in equation (6).

L = length, ft.
L_K = flow length of Krischer, ft.
L' = characteristic length of Krischer and Loos, ft.
L'' = new characteristic dimension, ft.
P = perimeter of a shape, ft.
P_{LM} = log mean pressure difference of air across the boundary layer, atmosphere.
q = heat transferred, B.t.u./hr.
s = average humid heat of the gas film, (B.t.u.)/(lb. dry air)(°F.).
t_f = arithmetic mean air film temperature, °F.
t_a = dry bulb air temperature, °F.
T_b = absolute temperature of bulk air flow, °R.
T_s = absolute temperature of particle surface, °R.

Greek Symbols

δ_s = thickness of velocity boundary layer, ft.
δ_T = thickness of thermal boundary layer, ft.
μ_f = average viscosity of air film, lb. mass/(ft.)(hr.).
ρ_f = average density of air film, lb./ft.[3]
λ = Leva's shape factor, dimensionless.
ϕ_s = Carman's shape factor, dimensionless.
ψ = Wadell's sphericity = A_p/A, dimensionless.

Dimensionless Groups

j'_D = Mass transfer factor = $(k_G P_{LM}/G_m)(\mathrm{Sc})^{2/3}$
j_H = Heat transfer factor = $(h/c_p G)(\mathrm{Pr})^{2/3}$
Nu = Nusselt Number = hd/k_f (for spheres) or hL''/k_f
Nu' = Nusselt Number for mass transfer = $k_G M L'' P_{LM}/D_v \rho_f = Nu\,(k_f/s D_v \rho_f)$
Pr = Prandtl Number for heat transfer = $c_p \mu_f/k_f$
Re = Reynolds Number for spheres = dG/μ_f
Re' = Reynolds Number = $L''G/\mu_f$
Re_p = Reynolds Number = PG/μ_f (equation 4)
Sc = Schmidt Number for mass transfer = $\mu_f/D_v \rho_f$

References

(1) Bar-Ilan, M., and Resnick, Ind. Eng. Chem., **49**: 313 (1957).
(2) Cadle, R. D., "Particle Size Determination", Interscience Publishers Inc., New York and London (1955).
(3) Gebelein, H., Chem.-Ing.-Tech., **30**: 594 (1958).
(4) Herdan, G., and Smith, M. L., "Small Particle Statistics", Elsevier Publishing Co., New York (1953).
(5) Wadell, H., J. Franklin Inst., **217**: 459 (1934).
(6) Carman, P. C., Trans. Inst. Chem. Eng. (London), **15**: 150 (1937).
(7) Leva, M., et al., "Fluid Flow through Packed and Fluidized Systems", U.S. Bureau of Mines, Bull. 504, U.S. Govt. Print. Off., Washington (1951).
(8) Powell, R. W., Trans. Inst. Chem. Engrs. (London), **18**: 36 (1940).
(9) Krischer, O., and Loos, G., Chem.-Ing.-Tech., **30**: 31 (1958).
(10) Ibid, p. 69.
(11) Ranz, W. E., and Marshall, W. R., Chem. Eng. Progr., **48**: 173 (1952).
(12) Chilton, T. H., and Colburn, A. P., Ind. Eng. Chem., **26**: 1183 (1934).
(13) Linton, W. H., and Sherwood, T. K., Chem. Eng. Progr., **46**: 258 (1950).
(14) Maisel, D. S., and Sherwood, T. K., Chem. Eng. Progr., **46**: 131 (1950).
(15) Ibid, p. 172.
(16) Krischer, O., Chem.-Ing.-Tech., **25**: 738 (1953).
(17) Krischer, O., "Die Wissenshaftlichen Grundlagen der Trocknungstechnik", Vol. 1, p. 123, Springer-Verlag, Berlin (1956).
(18) Washburn, E. W. (editor-in-chief), "International Critical Tables", Vol. 5, 1st ed., p. 62, McGraw Hill Book Co. Inc., New York (1929).
(19) Williams, G. C., D.Sc. Thesis (Chem. Eng.), Massachusetts Inst. of Technology (1942).
(20) Brown, R. A. S., Sato, K., and Sage, B. K., Ind. Eng. Chem., Data Series, **3**: 263 (1958).
(21) Schnautz, J. A., Ph.D. Thesis (Chem. Eng.), Oregon State College (1958).
(22) Van de Hegge Zijnn, B. G., Appl. Sci. Research, **A 7**: 205 (1958).
(23) Cary, J. R., Trans. Am. Soc. Mech. Engrs., **75**: 483 (1953).
(24) Garner, F. H., Chem. and Ind., No. 8, 141 (1956).
(25) Robinson, W., and Han, L. S., Proc. 2nd Mid-Western Conf. Fluid Mech., Bull. 149, Ohio State Univ. Studies, Eng. Ser. 3, **21**: 349 (1952).
(26) Winding, C. C., and Cheney, A. J., Ind. Eng. Chem., **40**: 1087 (1948).
(27) Perry, J. H. (editor-in-chief), "Chemical Engineers' Handbook", 3rd ed., p. 545, McGraw-Hill Book Co. Inc., New York (1950).
(28) Pasquill, F., Proc. Roy. Soc. (London), **A 182**: 75 (1943).
(29) Wade, S. H., Trans. Inst. Chem. Engrs. (London), **20**: 1 (1942).
(30) Pohlhausen, K., Z. angew. Math. Mech., **1**: 252 (1921).
(31) Latzko, H., Nat. Adv. Comm. Aero. Tech. Memo 1068 (1944).
(32) Norris, R. H., and Spofford, W. A., Trans. Am. Soc. Mech. Engrs., **64**: 489 (1942).
(33) Fage, A., and Falkner, V. M., G. Brit. Aero Res. Comm. Tech. Rept. and Memo 1408, 39, 172 (1931).
(34) Colburn, A. P., Trans. Am. Inst. Chem. Engrs., **29**: 174 (1933).
(35) Grimison, E. D., Trans. Am. Soc. Mech. Engrs., **59**: 583 (1937).
(36) Hilpert, R., Forsch. Gebiete Ingenieurw., **4**: **215** (1933).
(37) Schlichting, H., "Boundary Layer Theory", 1st ed., McGraw-Hill Book Co. Inc., New York (1955).

★ ★ ★

The Effect of Temperature on the Fluidization of Silver Powders[1]

E. ECHIGOYA[2] *and G. L. OSBERG*[3]

Fluidization tests on pure silver and silver catalyst powder show that agglomeration occurs when the bed is heated, which finally results in bed collapse at a comparatively low temperature. If the bed temperature is held constant in the agglomerating temperature range, an induction period is observed before fluidization ceases. A study of the induction period as a function of temperature (10-60°C.) leads to an activation energy of 18 kcal. for the overall agglomeration process for pure silver. Agglomeration is believed to be due to sintering.

Interest in these laboratories in fluidized silver powders developed from exploratory design studies on catalysts prepared from *Ca Ag* alloys (1) which have been proposed for the oxidation of ethylene to ethylene oxide. Small scale fluidizing tests with these catalysts showed that the formation of agglomerates, when the bed temperature was raised, prevented stable fluidization in the operating temperature range. When fluidization ceased, catalyst tempeartures were uncontrollable because of poor heat transfer. Since little information has appeared on the agglomeration of fluidized metal powders, it is perhaps of interest to summarize our observations on fluidized silver powder systems.

Experimental Method

The fluidizing tests were carried out in a 2.5 cm. I.D. or 5 cm. I.D., electrically heated, pyrex tube with a conical (23° included angle) bottom through which the fluidizing gas was fed. The inlet gas passed through a drying tube and rotameter, and the outlet gas through a cyclone. A manometer was connected to the bottom of the cone, and to the top of the pyrex tube, so that pressure drop measurement could be taken across the bed. Bed temperatures were measured with a thermocouple dipping into the bed.

Fluidizing difficulties due to agglomerate formation were directly visible through the pyrex tube, but were also readily deduced from pressure drop readings. With normal fluidization, pressure drop readings fluctuated slightly, but with the mean value equal to the weight of the bed. As agglomeration occurred, parts of the bed were immobilized; channels developed through the bed, causing a sudden decrease in pressure drop. Under some conditions these large erratic fluctuations were repeated several times before the bed was completely immobilized.

[1]*Manuscript received July 21, 1959; Accepted December 7, 1959.*

[2]*N.R.C. Postdoctorate Fellow. Present address: Tokyo Institute of Technology, Ookayama, Meguro-Ku, Tokyo, Japan.*

[3]*Division of Applied Chemistry, National Research Council, Ottawa, Ont. Contribution from Division of Applied Chemistry, National Research Council, Ottawa, Ont. Issued as N.R.C. No. 5562.*

Powder samples used in these experiments were silver powder and silver catalyst. The silver powder was of high purity containing .0005% *Pb*, .005% SiO_2 .0004% *Fe*, .0002% *Al*. The silver catalyst was prepared from 8.5% *Ca*, 91.5% *Ag* alloy powder as described by McKim and Cambron (1). The calcium was removed by leaching with 20% acetic acid after pre-treatment for one hour with water in an autoclave at 225°C. Following leaching, washing and drying, a catalytically-active silver catalyst was obtained having a residual calcium content of about 0.15% and a specific surface area of 0.5 sq. m./gm.

Observations

At room temperature silver catalyst powders fluidized satisfactorily in air, but when heated ceased to fluidize at a definite temperature. In Figure 1, the arrest temperatures are given for three mesh sizes (Tyler) of silver catalyst. It may be noted that the finer powders show substantially lower arrest temperatures, and that air flow rates within the range shown had only a minor effect. A separate series of tests with sample sizes varying from 10-25 cc. in the 2.5 cm. I.D. tube, showed no significant effect of volume of sample on the arrest temperature observed.

The agglomerates which formed at these low temperatures were of relatively low strength. Cooling the bed to room temperature, and maintaining the gas flow was often sufficient to bring about fluidization again. If this cycle of heating and cooling was repeated several times, however, a lower temperature was observed after each cycle though the arrest temperature appeared to be tending toward a constant value.

Induction Period

When a fresh sample of powder was maintained at a constant temperature under fluidizing conditions difficulties due to agglomeration did not occur immediately. A time interval was observed which depended on the bed temperature. An induction period was therefore selected as the time interval between the beginning of fluidization, and the first major decrease in pressure drop which culminated in bed immobility. Induction periods, thus defined, were observed with pure silver, and with silver catalyst powders using air, hydrogen and argon as fluidizing gases. When hydrogen was used there was no difficulty in observing the induction period because bed immobility occurred immediately after the first major decrease in pressure. When air or argon was used, major pressure fluctuations were erratic and occurred several times, with normal readings in between, before fluidization finally ceased. For this reason, the first major fluctuation in the series which culminated in immobilization of the bed was arbitrarily selected as marking the end of the induction period.

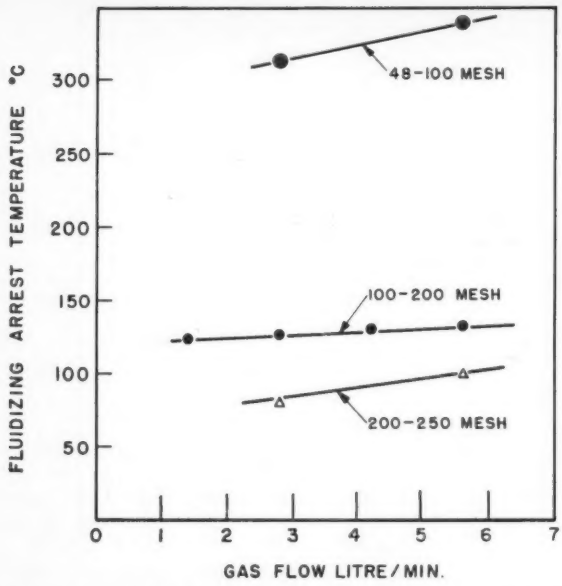

Figure 1 — Fluidizing arrest temperatures for different mesh ranges of silver catalyst in air in a 2.5 cm. I.D. fluidizer.

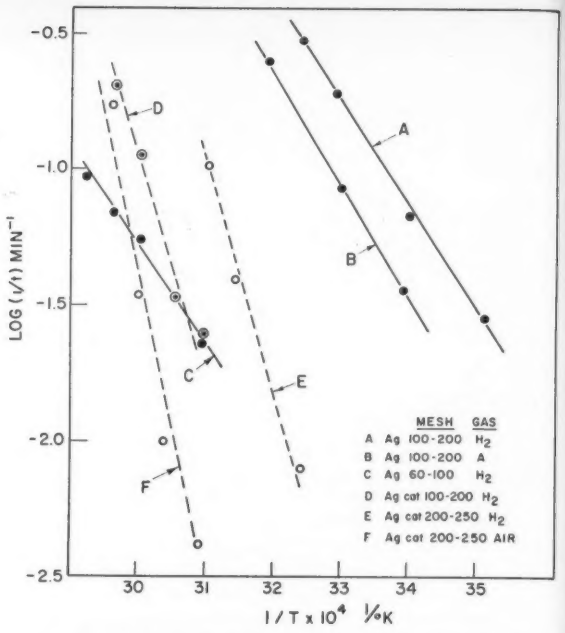

Figure 2—Induction period vs reciprocal temperature.

The quality of fluidization also had an effect on the observed induction period. When slugging conditions were encountered, longer induction periods were observed. With small bed volumes, i.e. 5 to 12 cc., slugging was not encountered, and reproducible induction periods were obtained.

Induction period data are given in Figure 2 for a temperature range of 10 to 60°C. These bed temperatures were obtained by immersing the glass fluidizer in a constant temperature water bath. Bed sample size (10 cc.) and gas flow rates were constant for a particular set of temperature data. Gas flow rates at N.T.P. to the 2.5 cm. I.D. fluidizer were 2.8 litre/min. for air and argon, and 3.7 litre/min. for hydrogen.

The Arrhenius plot satisfactorily correlated the induction period as a function of reciprocal bed temperature so that the data may be represented by an empirical equation

$$\frac{1}{t} = A\, e^{-\Delta E/RT}$$

where t is the induction period, min., T is the bed temperature, °K., and A and E are experimental constants. Using the usual Arrhenius interpretation, ΔE is regarded as the activation energy for the overall agglomeration process.

Two groups of approximately parallel lines are shown in Figure 2. Plots A, B, and C were obtained with pure silver as the bed material. These have approximately the same slope, but have different intercepts. Changes in particle size, fluidizing gas and history of pure silver caused variations in the intercept, i.e. constant A. Changes in quality of fluidization which were obtained by using a 5 cm. I.D. glass unit instead of the 2.5 cm. I.D. unit reported here, also caused a change in the value of the intercept but not in the slope. The slope corresponds to an activation energy of about 18 kcal.

The second group of lines, D. E., and F, were obtained with silver catalyst as the bed material. Lines D and E are almost parallel while F is somewhat steeper. All are at a steeper slope than those for pure silver. The effect of mesh size, etc., is as above reflected in the intercept. The activation energy calculated from slope of these lines varies from 38 to 52 kcal.

Discussion of Data

It is evident from these limited data that the overall agglomeration process is a complex one. Fluidizing variables such as gas velocity, particle size, column design, etc., as well as surface properties of the metal powders all have an effect on the observed agglomeration rate, and no attempt is made to develop general correlations.

The formation of agglomerates is believed to be due to low temperature sintering of particles when these particles come into contact following collision within the fluidized bed. Low temperature sintering of metal powders is well known, and has been studied by Tammann and Mansuri [2] in a similar way, by noting the temperature at which stirrer ceases to move when stirring a metal powder which is being heated. They report arrest temperatures for silver in the range of 136-145°C. Thus, the fluidized bed tests above may be regarded as a different technique, perhaps a more sensitive one, for establishing the onset of sintering.

The mechanism of sintering of metal powder under low stress has received limited study. Kuczynski [3] has suggested that there is a close connection between sintering and the process of self diffusion. He observed experimentally that the rate of interfacial growth between a copper sphere in contact with a copper sheet is determined by the volume diffusion rate at high temperatures and predominantly by a surface diffusion mechanism at a low temperature.

Following this suggestion, it is interesting to compare the observed activation energy of 18 kcal. for agglomerating pure silver powder with published values of diffusion processes in silver. Hoffman and Turnbull [4] report an activation energy of 20.2 kcal. for grain boundary data obtained on polycrystalline silver at 400°C. They give a value of 45.9 kcal. for the lattice diffusion rate in a single

crystal of silver. Nickerson and Parker [5] report an activation energy of 10.3 kcal. for the surface diffusion of silver. The activation energy obtained from the agglomeration data is intermediate between the surface and lattice diffusion values, and rather close to the grain boundary diffusion value. The activation energy of 38-50 kcal. for silver catalyst would appear to be higher than for pure silver because of the presence of the impurity CaO, which might be regarded as hindering the mobility of the diffusing silver. The data presented here are, however, too limited to justify detailed speculations on the mechanism of sintering.

Minimizing Agglomerate Formation

These data show that the effect of agglomerate formation on fluidization can be minimized if coarse rather than fine silver particles are used, and if surface impurities such as CaO are present. Attempts have been made to render the silver catalysts non-agglomerating by the addition of diluent powders such as graphite as proposed by Sears [6], by the addition of small amounts of $CaCO_3$ [7], and by modification of the basic calcium silver alloy through the addition of hardening elements such as nickel. All these methods have been effective to a degree in overcoming agglomeration, but none, so far, have been completely satisfactory from both the fluidizing, and the catalytic point of view.

References

(1) McKim, F., Cambron, A., U.S. Pat. 2,562,857 (1951). Can. Pat. 475,366 (1951).
(2) Tammann, G., Mansuri, O. A., Anorg. Allgem. Chemie **126,** 119 (1923).
(3) Kuczynski, G. C., Journal of Metals **1,** 169 (1949).
(4) Hoffman, R. E., Turnbull, D., J. Appl. Phys. **22,** 634 (1951).
(5) Nickerson, R. A., Parker, E. R., Trans. Am. Soc. Metals **42,** 376 (1950).
(6) Sears, G. W., U.S. Pat. 2,615,899.
(7) Osberg, G. L., U.S. Pat. 2,537,486.

* * *

Edmonton, Alta.

Editor, C.J.Ch.E.:

We wish to point out the following errors which appeared in the February 1959 issue of the C.J.Ch.E. We thank B. C. Sakiadis of E.I. Du Pont de Nemours and Company for bringing them to our attention.

1. In the article "Horizontal Pipeline Flow of Mixtures of Oil and Water" by T. W. F. Russell, G. W. Hodgson and G. W. Govier, the term 8ay in the definition of M_2 in the Nomenclature should read 8ay3.

2. In the article "The Effect of the Less Viscous Liquid in the Laminar Flow of Two Immiscible Liquids" by T. W. F. Russell and M. E. Charles the term 8ay in the definition of M_2 in Equation (7) should read 8ay3 and the terms $(3\mu_A^2 + 6\mu_B + 11\mu_A\mu_B)\ a^2y^2$ in the equation between Equations (9) and (10) should read $4(3\mu_A^2 + 6\mu_B^2 - 11\mu_A\mu_B)a^2y^2$.

G. W. Hodgson and M. E. Charles,
Research Council of Alberta.

A Method for the Determination of Tie-Lines in Ternary Liquid Systems[1]

E. L. HERIC[2] and RONALD M. RUTLEDGE[3]

A method is described for the determination of tie-lines in ternary liquid systems which may be used when a satisfactory method of chemical analysis is unavailable. The technique is graphical and is based upon the lever rule principle. The method is illustrated with the system acetic acid-furfural-water at 25 ± 0.05°. Results indicate the method is accurate and capable of good precision.

In a study of the system acetic acid-furfural-water in a manner rather more refined than those used previously[1,2], a suitable method was needed for the determination of the tie-lines. Usually the presence of an acid as one of the components suggests titration of that component with a base as the simplest method. In the present instance, however, it was felt that this method might not be feasible because of the instability of furfural[3,4]. It was thought that the acidic nature of some of the decomposition products might introduce a systematic error if the method of tie-line determination were based upon acid titration.

There are available several methods of tie-line determination based upon the lever rule of Miller and McPherson[5]. The methods of Evans[6] and Othmer and Tobias[7] both require a knowledge of the total weights of a synthetic sample and each of the conjugate phases formed from the sample. Another technique described by Bancroft and Hubard[8] involves working with only a representative fraction of each of the conjugate phases. Johnson and Barry[9], using a mechanical device, modified the latter method by eliminating some of its undesirable time-consuming trial and error features. While the approach of Johnson and Barry is convenient, it was hoped that our data would be of sufficient precision to warrant the use of a larger graphical scale for evaluation, rendering the size of their mechanical device impractically large. The method described in this paper is another approach to modification of the method of Bancroft and Hubard, again removing its trial and error features but requiring no mechanical device other than a straight-edge.

Chemicals and Equipment

Furfural, commercial grade, was purified by distillation under vacuum, and only the middle fractions were used. For freshly distilled furfural, n_D at 25 ± 0.05° was 1.5235. The accepted value is 1.52345[10]. To minimize decomposition of the furfural during storage, it was kept in closed containers at the sublimation temperature of carbon dioxide. When used, each sample of furfural was colorless, although a slight coloration was frequently evident by the time the sample was discarded. Acetic acid was of reagent grade quality, minimum assay 99.7% by weight. It was used without further purification. Water was from a laboratory still. The thermostated samples were maintained at a temperature of 25 ± 0.05°.

Determination of the Binodal Curve

The binodal curve was determined by adding acetic acid to synthetic samples in the two-phase region until homogeneity was established. From the weights of the three components present, points on the curve were established. Because of the instability of furfural only one or, at the most, two points on the curve were established with a given sample of furfural. While duplicate determinations were not made for three-component samples, an indication of the precision of this work is given by the results obtained in repeated determinations of the solubilities of furfural in water and water in furfural. In both the former, where three determinations were made, and the latter, where four determinations were made, the average deviations were less than 0.1% by weight. The solubility curve of the system is given in Figure 1.

In passing, a remark concerning the effect of furfural decomposition on solubility is pertinent here. It has been found that the decomposition of furfural has little effect on solubility in some instances[11]. However, when compared with the present work, data obtained by one of the authors previously[12] on the solubility of furfural in water and vice versa (with less carefully purified furfural than used here) shows sufficient disagreement with the present work to throw doubt upon the generality of such an assumption.

Determination of the Tie-Lines

Tie-line determination was accomplished with the aid of Figures 2 and 3. The former is a reconstruction of Figure 1 in terms of a right triangle*, and is necessary because the scale of the usual equilateral triangular graph paper is too small for precise work. By adopting a right triangle it is possible to use an extended form of rectangular coordinate paper, giving a higher degree of sensitivity to the method. (Figure 2 has been drawn out of scale in order to show more clearly the essential features of the method.)

Points K and L in Figure 2 represent two binary mixtures of respectively acetic acid and furfural, and acetic acid and water. From K a number of straight lines were drawn through the binodal curve, such as KN_1Z_1, KN_2Z_2 and KN_3Z_3. The locations of the points such as Z_1, Z_2, Z_3 are arbitrary, except that

[1]*Manuscript received August 19, 1959; Accepted January 15, 1960.*

[2]*Assistant Professor, Department of Chemistry, University of Georgia, Athens, Georgia.*

[3]*Present address: Department of Chemistry, University of Tennessee, Knoxville, Tennessee.*

*In practice the construction of Figure 1 is not necessary for the application of the method to be described. It is used here only as a means of presenting the data of the system in the more usually encountered form.

in the present system, for example, they were to cover the range of solutions found on the water-rich portion of the binodal curve. In a like manner straight lines were drawn through the binodal curve from point L, such as Y_1M_1L, Y_2M_2L and Y_3M_3L. Again the locations of the points such as Y_1, Y_2, Y_3 are arbitrary, except that in the present system they were to cover the range of solutions found on the furfural-rich portion of the binodal curve. Because of the arbitrary way in which the Y and Z points have been selected, it is apparent that like subscripts on a pair of points Y and Z do not infer that these points bear any relationship to one another. At each of the points N and Z on a given line KNZ the weight percentages of water, W_N and W_Z, were read from Figure 2 and recorded. It was thus possible to construct the curve in Figure 3 of W_N/W_Z versus W_Z. Similarly at each of the points Y and M on a given line YML the weight percentages of furfural, F_Y and F_M, were read from Figure 2 and recorded. The curve in Figure 3 of F_M/F_Y versus F_Y was then constructed. By combining the information in Figure 3 with the experimental procedure described next, it was possible to determine the tie-lines of the system.

A series of synthetic samples were prepared. Each sample separated into two conjugate phases, Y and Z, whose compositions were to be determined. A fraction of each of the two phases in each sample was removed and titrated with a titrant solution. The composition of the titrant solution corresponded to either K or L in Figure 2. Solution K, containing 20.0 weight % acetic acid and 80.0 weight % furfural, was used to titrate those fractions on the water rich side of the binodal curve, the Z phases. Solution L, containing 20.0 weight % acetic acid and 80.0 weight % water, was used to titrate those fractions on the furfural rich side of the binodal curve, the Y phases. In every case the fractions were titrated to clearness following the initial formation of a cloudy suspension. At the "end points" of the titrations the compositions of the titrated fractions were points M and N on the opposite side of the binodal curve from the fraction being titrated. M and N lie on the straight lines joining L and Y in the one instance, and K and Z in the other.

By the lever rule, if to a weight g_Z of composition Z there is added a weight g_K of composition K in order to achieve a composition of N, then

$$\frac{g_K}{g_Z} = \frac{\overline{NZ}}{\overline{KN}} \qquad (1)$$

Moreover it follows from Equation (1) that

$$\frac{g_Z}{g_K + g_Z} = \frac{\overline{KN}}{\overline{KZ}} \qquad (2)$$

In addition, as has been discussed elsewhere[13], it follows that

$$\frac{\overline{KN}}{\overline{KZ}} = \frac{W_N - W_K}{W_Z - W_K} \qquad (3)$$

Now since K lies on the acetic acid axis W_K is zero, so from Equations (2) and (3)

$$\frac{g_Z}{g_K + g_Z} = \frac{W_N}{W_Z} \qquad (4)$$

By a similar argument it can be shown that for points Y on the furfural-rich side

$$\frac{g_Y}{g_L + g_Y} = \frac{F_M}{F_Y} \qquad (5)$$

It follows that experimental determination of

$$\frac{g_Z}{g_K + g_Z} \text{ and } \frac{g_Y}{g_L + g_Y}$$

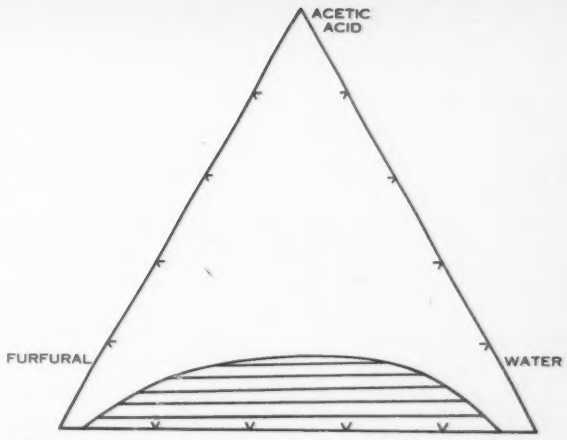

Figure 1—The system acetic acid-furfural-water at 25°.

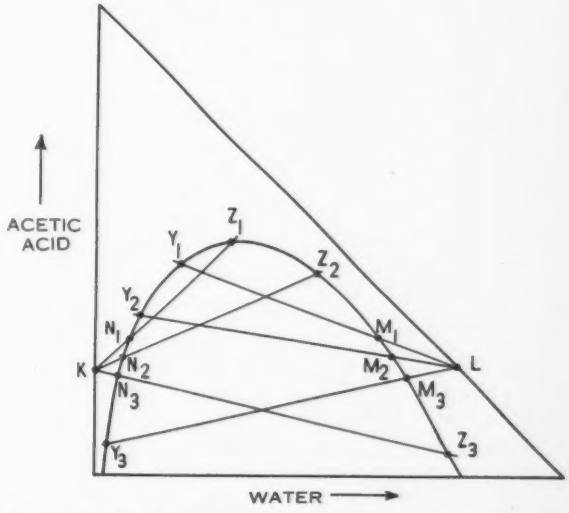

Figure 2—An illustration of the method used in constructing the working plot for tie-line determination.

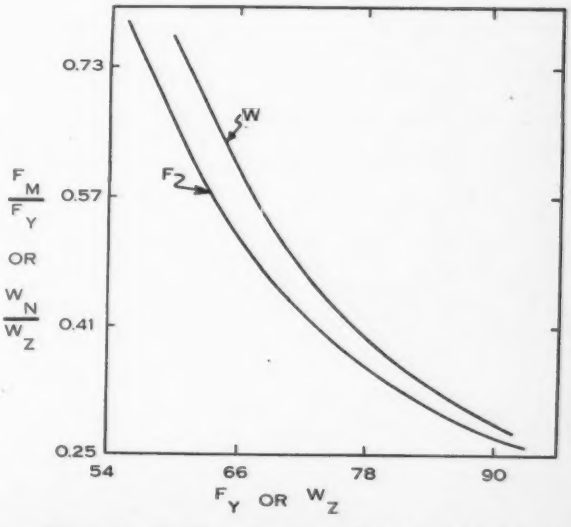

Figure 3—Working plot for tie-line determination.

TABLE 1

TIE-LINE DATA AT 25° (IN PER CENT BY WEIGHT)

Furfural rich phase			Water rich phase			Tie-line error
Water	furfural	acetic acid	Water	furfural	acetic acid	(See text)
7.2	89.9	2.9	87.2	9.3	3.5	+0.2
9.6	85.0	5.4	82.1	11.3	6.6	±0.0
12.6	79.4	8.0	76.4	14.1	9.5	−0.1
17.1	71.9	11.0	69.2	18.1	12.7	−0.1
24.9	60.9	14.2	59.2	25.2	15.4	±0.0

is sufficient to fix a tie-line, since these quantities are identical to respectively W_N/W_Z and F_M/F_Y. A knowledge of the values of these latter functions leads directly to the corresponding values of W_Z and F_Y for a pair of conjugate solutions, using Figure 3.

As an illustration of the method the following example is given for a pair of conjugate phases at equilibrium:

$$g_Z = 18.89 \text{ g.}$$

$$g_K = 16.50 \text{ g.}$$

$$\frac{g_Z}{g_K + g_Z} = \frac{W_N}{W_Z} = 0.534$$

$$g_Y = 27.96 \text{ g.}$$

$$g_L = 37.98 \text{ g.}$$

$$\frac{g_Y}{g_L + g_Y} = \frac{F_M}{F_Y} = 0.424$$

Thus from Figure 3, W_Z is 69.2%, and from Figure 2 the corresponding values of the furfural and acid concentrations at this point on the binodal curve are respectively 18.1 and 12.7 %. Again using Figures 3 and 2, F_Y is 71.9%, and the corresponding values of the water and acid concentrations at this point on the binodal curve are respectively 17.1 and 11.0%.

Five tie-lines were determined in this manner. The results are given in Table 1. In order to determine the accuracy of the method the compositions of the synthetic samples in the two-phase region used in determining conjugate phase compositions were recorded. For absolute accuracy each tie-line should pass precisely through the point representing the composition of the synthetic sample used in determining the tie-line. The amount whereby the tie-line missed each such point at its closest approach is also given in Table 1 in terms of % by weight of acetic acid. This is a convenient method of describing the quality of the data in the present system since the tie-lines are essentially parallel to the water-furfural axis. The average amount by which a tie-line misses passing through the synthetic sample point is slightly less than 0.1% acetic acid. The agreement is sufficient to establish that the method is practical. In practice a knowledge of the composition of the synthetic samples would not be necessary in order to determine the tie-lines by this method, but the slight amount of extra labor involved appears to be worthwhile when one considers the means it provides for checking one's accuracy.

It should be noted that for best results points K and L must be selected so that in terms of the consolute liquid they contain somewhat less than the maximum concentration of that component on the binodal curve. Otherwise for points near the top of the binodal curve the addition of neither K nor L will produce a locus of points passing through the two-phase region. The latter, of course, is essential to the method described here. Another point of interest is that for some systems where the plait point is displaced considerably away from the maximum of the binodal curve, it may be necessary to titrate both of the conjugate phases with either K or L for tie-lines near the plait point. Such behavior may be anticipated by determining first those tie-lines near the base of the two-phase region and noting the trend of the tie-lines as the maximum of the binodal curve is approached.

It will be apparent from Figure 3 that the sensitivity of the method is not uniform over the entire range of the binodal curve. As F_M/F_Y or W_N/W_Z approaches unity the sensitivity decreases. Indeed, for any two working solutions such as K and L there will be a point of tangency to the binodal curve for each of the lines KNZ and YML. At such a point the method of this paper is not applicable. The region of the binodal curve subject to this difficulty is small, however, judging from the results presented here.

Acknowledgement

The Quaker Oats Chemical Company supplied the furfural used in this work.

Nomenclature

K, L, M, N, Y, Z = various points on the phase diagram (Figure 2), either on the binodal curve, the furfural-acetic acid axis or the water-acetic acid axis; specific points on the binodal curve are indicated by the subscripts 1, 2 or 3.

W_N and W_Z = the weight per cents of water at points N and Z on the binodal curve.

F_M and F_Y = the weight per cents of furfural at points M and Y on the binodal curve.

g_K, g_L, g_Y, g_Z = the weight of samples of solutions corresponding respectively to compositions K, L, Y or Z.

References

(1) Skrzec, A. C., and Murphy, N. F., Ind. Eng. Chem., **46,** 2245 (1954).

(2) Pegoraro, M., and Guglielmi, G., Chimica e industria (Milan), **37,** 1035 (1955).

(3) Dunlop, A. P., Stout, P., and Swadesh, S., Ind. Eng. Chem., **38,** 705 (1946).

(4) Williams, D. L., and Dunlop, A. P., Ind. Eng. Chem., **40,** 239 (1948).

(5) Miller, W. L., and McPherson, R. H., J. Phys. Chem., **12,** 710 (1908).

(6) Evans, T. W., Ind. Eng. Chem., Anal. Ed., **6,** 408 (1934).

(7) Othmer, D. F., and Tobias, P. E., Ind. Eng. Chem., **34,** 690 (1942).

(8) Bancroft, W. D., and Hubard, S. S., J. Am. Chem. Soc., **64,** 347 (1942).

(9) Johnson, A. I., and Barry, T. W., Can. J. Technol., **32,** 17 (1954).

(10) Walden, P., Z. Physik. Chem., **59,** 394 (1907).

(11) Lloyd, B. A., Thompson, S. O., and Ferguson, J. B., Canadian J. Res., **15 (B),** 98 (1937).

(12) Heric, E. L., Chemist-Analyst, **48,** 31 (1959).

(13) Morey, G. W., J. Phys. Chem., **34,** 1745 (1930).

* * *

Machine Computations for Transient Stagewise Processes[1]

D. YESBERG[2] and A. I. JOHNSON[3]

A review of recent work on transient stagewise mass transfer processes is presented, with particular emphasis on numerical and analog solutions for the partial differential difference equations involved. The numerical or analog solutions are relatively simple, whereas the analytical solution even of the linearized equation is quite involved.

An example of gas absorption is considered in which the equations are linearized, and solved numerically as well as by the use of a resistance network analog. These particular methods of solution had not previously been used for this problem, and the present work is compared with previous solutions. The novel feature of the method of solution is the representation of the time derivative by a backward finite difference to produce a set of simultaneous algebraic equations, which may be solved most easily by matrix inversion programmed on a digital computer.

It has been pointed out by many authors that a great deal of research remains to be done before completely automatic chemical plants become a reality[1]. One of the tools available for the study of problems in the instrumentation of automatic plants is the electronic analog computer. Using this instrument, process equipment may be simulated electrically and the control characteristics of such process equipment investigated in the laboratory. Besides being useful for the study of control problems, an electrical analog of such mass transfer equipment as distillation, extraction or absorption towers is useful for predicting the time of approach to steady state such as occurs at the start-up of the equipment.

This paper discusses a resistance network analog for a gas absorption tower, and its use for predicting the rate of approach to steady state. The analog was developed by Liebmann[2] for solving the heat conduction or diffusion equation.

Transient Stagewise Processes

In 1940 several authors discussed transient mass transfer in batch fractionation [3, 4, 5, 6, 7]. However it was not until Marshall and Pigford published their book in 1947[8] that the concept of transient behavior in stagewise processes was thoroughly developed. Lapidus and Amundson[9] extended the special case considered by Marshall and Pigford to a complete solution of the transient and unsteady state for a general linear equilibrium relation such as is found in absorption and extraction problems, and for constant feed rates. The use of a linear equilibrium relation restricted the application of the derived formulae to limited ranges of concentration changes, but the authors felt that qualitative conclusions for the non-linear cases could be drawn from the results obtained. Their equation, obtained by a mass balance on the m th stage was

$$H\frac{\partial Y_m}{\partial t}(t) + h\frac{\partial X_m}{\partial t}(t) = L\,X_{m-1}(t) + X_m(t) + G\,Y_{m+1}(t) - Y_m(t) \quad \ldots\ldots(1)$$

and by the use of the equilibrium relation

$$Y_m(t) = \alpha\,X_m(t) + \beta \quad \ldots\ldots(2)$$

results in

$$(H\alpha + h)\frac{\partial X_m(t)}{\partial t} = LX_{m-1}(t) - (L + G\alpha)X_m(t) + G\alpha X_{m+1}(t) \quad \ldots\ldots(3)$$

The conditions at the two ends of the column are described by

$$X_o(t) = f(t) \text{ when } m = O \text{ (upper end)} \quad \ldots\ldots(4)$$

$$Y_{M+1}(t) = g(t) \text{ when } m = M+1 \text{ (lower end)} \quad \ldots\ldots(5)$$

and the condition of the column at t = 0 is given by

$$X_m(O) = A_m \quad \ldots\ldots(6)$$

The Equations (3), (4), (5), (6) make up a complete mathematical description of the problem, and it is the solution of this problem which must be found.

In 1951, Pigford, Tepe and Garrahan[10] solved the equations similar to[1] as applied to batch rectification using a mechanical analog computer at the University of Pennsylvania, and did not need to limit themselves to a linear vapor-liquid equilibrium relation.

In 1953, Rose et al.[11] published a detailed summary of their work over the preceding 13 years on the theory of batch rectification. Also in 1953, Acrivos and Amundson[13] published solutions for the problem Lapidus and Amundson[9] had first considered in 1950. This time[13] a Reeves Electronic Analog Computer (REAC) was used to find solutions for both linear and non-linear vapor-liquid equilibrium relations. Acrivos and Amundson [14] considered yet another method of solution using matrix methods.

In 1955, Rose and Williams [15] used a REAC to solve the problem of transients in continuous distillation, for constant relative volatility. They also introduced the dynamic characteristics of the stagewise system into the solution, and showed how these solutions could determine the most satisfactory method of instrumental control. This investigation was continued in a later paper [16].

[1]*Manuscript received October 21, 1959; Accepted January 26, 1960.*
[2]*Graduate student, Department of Chemical Engineering, University of Minnesota.*
[3]*Associate professor, Department of Chemical Engineering, University of Toronto, Toronto, Ont.*
Contribution from the Department of Chemical Engineering, University of Toronto, Toronto, Ont. Based on a paper presented to C.I.C. Chemical Engineering Conference, November 9-11, 1959.

In 1956, Jackson and Pigford [17] considered the rate of approach to steady state in a distillation column. These authors replaced the finite difference terms of Equation (1) by the approximate differential quotient equivalents, and pointed out that the resulting partial differential equation was of the heat conduction type. An empirical correlation for the time of approach to steady state was derived using the results of computer calcuations.

In 1957, Mickley, Sherwood and Reed treated several transient stagewise processes in their book [18]. A particularly important contribution was made by Rosenbrock [19] who overcame the disadvantage of the finite difference method of solution of Rose et al. [11] by using a method similar to that developed by Crank and Nicolson [20] to solve the heat conduction equation. Rosenbrock used a digital computer to solve the equations and analyzed his reasons for using this equipment. He also listed clearly the idealizations and assumptions that he included in the computer program.

Rose, Sweeney and Schrodt [21] have presented an extension of the work of Rose et al [11] to include multicomponent continuous distillation calculations. However, as mentioned above, the feasibility of this method for predicting the rate of approach to steady state depends on the correct selection of the size of the time interval.

There have been a number of articles published concerning the transient behavior of packed columns, but these will not be considered.

Machine Solutions

The first machine solutions of the partial differential difference equation

$$\frac{\partial C'}{\partial T} = \frac{C'_{m-1} - 2C'_m + C'_{m+1}}{(\Delta x')^2} \qquad (7)$$

where (7) is written in terms of reduced length and time variables x' and T was solved by Hartree and co-workers [22] using a mechanical differential analyzer. They replaced the second order space derivative by the approximate finite difference expressions and then proceeded to solve each of the set of ordinary differential equations so formed. This method is still used with electronic differential analyzers, and a discussion is presented by Karplus [23, ch. 12].

Acrivos and Amundson [13] used an electronic differential analyzer to solve [3] using circuits very similar in principle to those used for the somewhat simpler diffusion equation approximation [7].

Another method of machine solution was suggested by Beuken in 1937 [24], where a direct electrical analogy of the diffusion equation may be obtained by considering the flow of current along a lumped cable. The electrical equation is derived in many texts e.g. [25], and for zero inductance, and zero leakage to earth from the lumped cable, the equation is

$$\frac{\partial V}{\partial t} = \frac{1}{RC}\left[\frac{V_{m-1} - 2V_m + V_{m+1}}{(\Delta x)^2}\right] \qquad (8)$$

where R is the resistance, and C is the capacitance per unit length of cable. A lumped resistance-capacitance network or cable is shown in Figure 1 for comparison with the Liebmann circuit to be discussed in this paper.

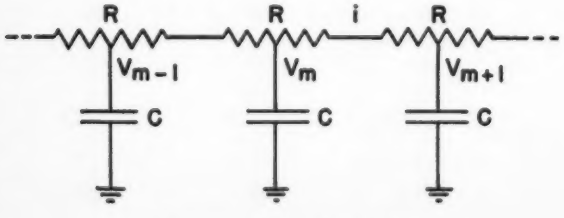

Figure 1—Lumped cable.

Paschkis [26] describes the construction of such an electrical analog. By a suitable choice of scale factors the electrical model may be operated at convenient voltages and time intervals and may be built with feasible magnitudes of resistance and capacitance. The possibility of being able to change the time scale is of paramount importance for the practicability of the method. A process taking days or hours can be condensed to a few minutes, and vice versa. Paschkis and Hlinka [27] have extended the versatility of this direct analog by the use of unity gain cathode followers [23, p. 256].

Liebmann [2] has devised a resistance network analog in which the time derivative of [8] is also approximated by finite differences. Liebmann's method of using backward differences [28] satisfactorily overcomes the criticism levelled at forward difference representation as used by Rose et al [11, 21]. Liebmann's analog is discussed in great detail by Karplus [23].

Time Derivative Approximation

For numerical solution of the partial differential difference Equation (3) the time derivative may be replaced by three different finite difference expressions.

$$\left[\frac{\partial X_m}{\partial t}\right]_n \doteq \frac{X_{m,n+1} - X_{m,n}}{\Delta t} \qquad (9)$$

$$\left[\frac{\partial X_m}{\partial t}\right]_n \doteq \frac{X_{m,n} - X_{m,n-1}}{\Delta t} \qquad (10)$$

$$\left[\frac{\partial X_m}{\partial t}\right]_n \doteq \tfrac{1}{2}\left[\frac{X_{m,n+1} - X_{m,n-1}}{\Delta t}\right] \qquad (11)$$

(X_m is the concentration on the m th tray at time $t = n\Delta t$.) Expressions (9) and (10) are forward and backward differences respectively. They have a somewhat larger truncation error for a given finite time interval than the Crank and Nicolson expression [11] [20] as mentioned by Crank [29, p. 137]

In 1928, Courant, Friedrichs and Lewy [30] called attention to the fact that in the numerical solution of equations such as (7) the choice of the size of the space interval Δx placed a restriction on the size of the time interval Δt when the forward difference expression (9) was substituted for the time derivative. This restriction does not apply to expressions (10) or (11). Von Newman [20, 31] has developed a method for determining whether this restriction applied to other formulae, while more elementary discussion of expressions (9) and (11) has been published by Rosenbrock [19], and Liebmann [28] has discussed expression (10).

Rose et al [11, 21] have used expression (9) extensively. Values of $X_{m,n+1}$ are determined successively by repeated application of the equation

$$\frac{(Ha + h)}{\Delta t}(X_{m,n+1} - X_{m,n}) = LX_{m-1,n} - (L + Ga)X_{m,n} + GaX_{m+1,n} \qquad (12)$$

to each stage, where the values of X_m at time $n\Delta t$ are known. However, as Rose has repeatedly pointed out, the size of the time interval is critical for stability of the solution.

Rosenbrock [19] has overcome the instability problem by using expression (11) to replace the finite difference on the left hand side of (12), while the present work uses expression (10), the backward difference, to give a set of simultaneous algebraic equations in $X_{m,n}$ ($m = 1 \ldots M$) as unknown, one equation for each stage.

$$\frac{Ha + h}{\Delta t}(X_{m,n} - X_{m,n-1}) = LX_{m-1,n} - (L + Ga)X_{m,n} + GaX_{m+1,n} \qquad (13)$$

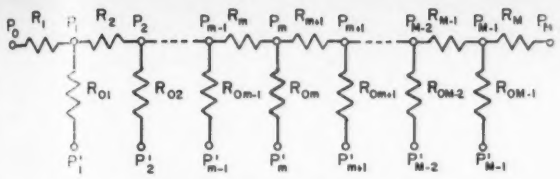

Figure 2—Resistance network.

These may be rearranged to

$$X_{m-1,n} - (1 + \theta + \phi)X_{m,n} + \theta X_{m+1,n} + \phi X_{m,n-1} = 0 \quad \ldots(14)$$

$$\text{where } \theta = \frac{G\alpha}{L} \text{ and } \phi = \frac{H\alpha + h}{L\Delta t} \quad \ldots(15)$$

Equation (14) may be solved using a resistance network, each solution giving the values of X_m for all stages at successive time intervals. The analog solutions may then be compared with numerical solutions.

The Resistance Network Analog of Liebmann

Consider a chain of M equal resistors R_m as in Figure 2. Let the beginning of this chain be P_0, the first junction point be P_1, etc., and the end point be P_M. The resistors will be called "network resistors". To each junction point $P_1, \ldots P_M, \ldots P_{M-1}$ a resistor of value R_{Om} is connected, the free ends of these resistors, called "series resistors", being the points $P'_1, \ldots P'_m, \ldots P'_{M-1}$. Let the value of R_{Om} be related to R_m by the formula

$$\theta = \frac{R_m}{R_{m+1}} \; ; \; \phi = \frac{R_m}{R_{Om}} \quad \ldots(16)$$

The chain of resistors R_m may then be considered a model of a stagewise operation. The junction points correspond to stages m = 0 . . . m = M in the real equipment, and P_0 and P_M correspond to the inlet streams. Let P_0 and P_M be connected to voltage sources V_0 and V_M corresponding to the prescribed inlet liquid concentrations X_0 and X_M, and let voltages $V_{1,0}, \ldots V_{m,0}$ corresponding to the prescribed initial concentrations $X_{1,0}, \ldots X_{m,0}$ be applied to the terminals ("feeding points") $P'_1, \ldots P'_m, \ldots$ of the series resistances R_{Om}. Then the voltages $V_{1,1}, \ldots V_{m,1}, \ldots$ will appear at the network junctions $P_1, \ldots P_m, \ldots$ and these voltages will correspond to the concentrations $X_{1,1}, \ldots X_{m,1} \ldots$ in the medium represented by the model at the time $t = \Delta t$.

If the network voltages $V_{m,1}$ are measured and the voltages at the feeding points P'_m made equal to $V_{m,1}$, then the voltages $V_{m,2}$ will appear at the network junctions corresponding to $X_{m,2}$ at the time $t = 2\Delta t$, and so on.

To prove this statement, consider the section of the network between the points P_{m-1} and P_{m+1} as shown in Figure 3.

According to Kirchoff's Law

$$\sum_{r=1}^{3} I_r = 0 \quad \ldots(17)$$

where I_1, I_2, I_3 are the currents flowing to the junction points P_m. Thus

$$V_{m-1,n} - \left(1 + \frac{R_m}{R_{m+1}} + \frac{R_m}{R_{Om}}\right) V_{m,n} + \frac{R_m}{R_{m+1}} V_{m+1,n} + \frac{R_m}{R_{Om}} V_{m,n-1} = 0 \quad \ldots(18)$$

which is formally identical with (14) provided (16) holds.

Hence the voltage relations in the described network model represent the difference Equation (14) within close limits set by the accuracy of the voltage measurements and the tolerances of the resistance values.

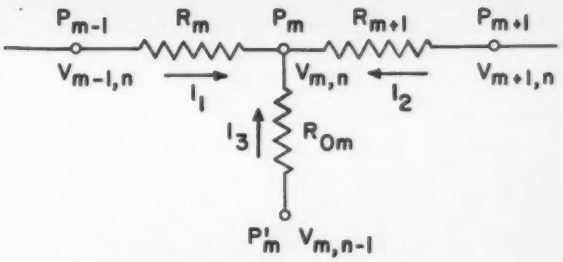

Figure 3—Liebmann analog element.

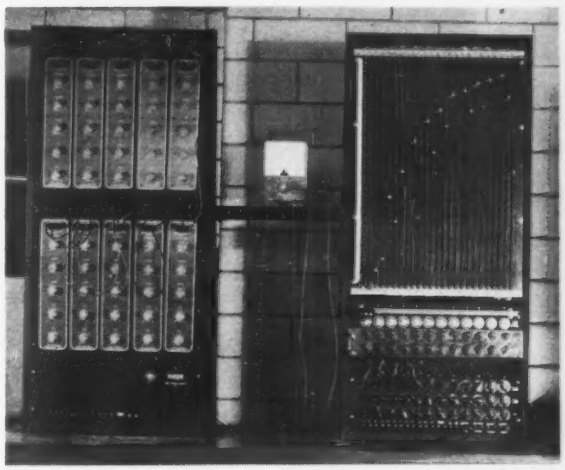

Figure 4—Photograph of Liebmann analog.

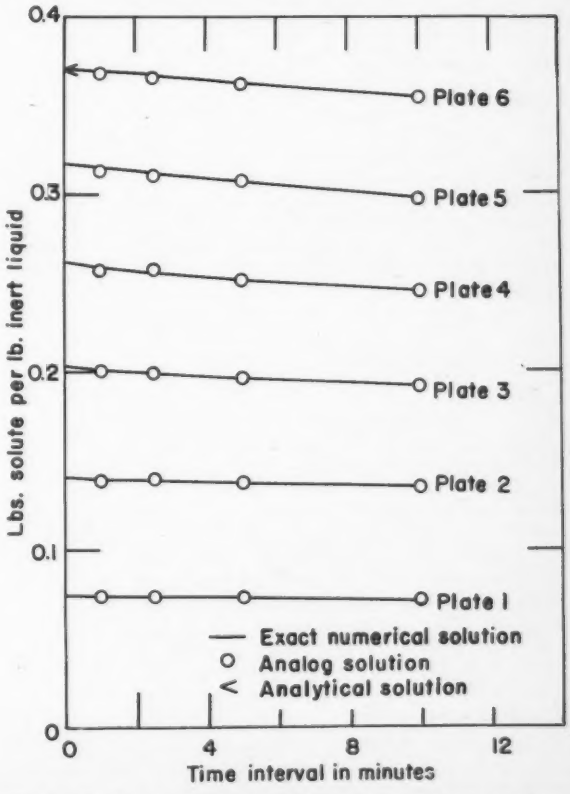

Figure 5—Comparison of analog and numerical solutions and illustration of the h^2 extrapolation.

The solution of the problem by the described analog model is subject to truncation errors of order Δt, but it is stable for any value of Δt, unlike solutions utilizing expression (9).

Apparatus

An apparatus similar to that of Liebmann [2] providing 11 network points was constructed, with provision made for use as two sets of six network points. It was assembled in two relay racks 44 inches high as shown in the photograph Figure 4. The relay rack on the left contained the resistance network, while the relay rack on the right contained the potentiometers, series resistors, and a set of resistors for allowing leakage to earth from the network points—"the leakage resistors". Further details may be found in Yesberg [32]. The use of the equipment may best be evaluated by considering a suitable numerical example.

Example of Gas Absorption

As a simple numerical example, Lapidus and Amundson (9) considered a six-plate column with solute component A in air and with water as the absorbent. The fat gas composition jumped from 0.2 lb. A per lb. of air to 0.3 lb. A per lb. of air. The problem is to determine how the fat solvent and lean gas compositions vary with time, and how long it takes to reach within 1% of steady state. Table 1 gives the required numerical data.

TABLE 1
GAS ABSORPTION EXAMPLE

Symbol	Numerical Value
a	0.72
β	0.0
G	66.7
L	40.8
h	75.0
H	1.0
$c = \frac{L}{Ga}$	0.85
M	6.0
X_o for all t	0.0
Y_{M+1}, $t = O$	0.2
Y_{M+1}, $t > O$	0.3
d	1.577

Lapidus and Amundson [9] first found the steady state values of A_m corresponding to $Y_{M+1} = 0.2$ by use of the steady state form of their solution to Equation (3). Table 2 gives these values of A_m.

TABLE 2
INITIAL STEADY STATE SOLUTION

$A_1 = 0.0613$	$A_4 = 0.1954$
$A_2 = 0.1135$	$A_5 = 0.2274$
$A_3 = 0.1578$	$A_6 = 0.2547$

With these steady state values known, the variation with time of X_6 the fat oil composition and Y_1 the lean gas composition can be found. It should be pointed out, however, that some transient values as presented in Lapidus and Amundson's Table 1 [9] were in error; but these errors were corrected in a later paper [13]. The correct values are presented in Table 3. The steady state fat oil and lean gas compositions can be shown to be 0.3821 and 0.0662 respectively.

Analog Computation

Four computations were performed on the analog to determine values of X for each tray ten minutes after a step change in the concentration of the entering fat gas stream had occurred. The time of ten minutes was chosen because it was known that the truncation errors would be significant at this time. The numerical coefficients for the sets of simultaneous equations, which determine also the ratio of values of adjacent resistors in the analog, are recorded in Table 4.

TABLE 3
SOLUTION OF GAS ABSORPTION EXAMPLE

Time	$X_m(t)$	$Y_1(t)$
0	0.2547	0.0441
1	0.3087	
3	0.3443	
5	0.3562	0.0497
10	0.3697	0.0558
15	0.3754	0.0604
20	0.3785	0.0830
25		0.0645
30		0.0653
35		0.0657
40		0.0660
45		0.0661
∞	0.3821	0.0662

TABLE 4
NUMERICAL COEFFICIENTS

Time Intervals	Δt Minutes	$\frac{Ga}{L}$	$\frac{Ha + h}{L\Delta t}$
1	10.0	1.177	0.1856
2	5.0	1.177	0.3712
4	2.5	1.177	0.7424
10	1.0	1.177	1.8560

Details of each of the first two computations are presented in full, the results of all four are plotted on Figure 5.

Notice that (14) and (15) are satisfied by the value of the resistances. The values for the initial steady state depend only on the values of the resistances R_m and the voltages applied at the ends of the network R_m. The difference between the expected values and the measured values is an indication of the accuracy of the component resistors and efficiency of the switches and potentiometers. Since the voltage across the potentiometers was approximately one volt, the voltage errors are of the order one to three millivolts. There are two concentrations of interest, the liquid composition on the bottom of the tray, and the gas composition leaving the top tray. For the purpose of comparing the numerical values, however, only the values of liquid composition on the bottom tray are presented.

Numerical Solution on a Digital Computer

To find the expected values of the voltages on the analog, numerical solutions of the sets of simultaneous Equation (14) were performed on an IBM 650 digital computer. A slight variation of the Fox and Thomas modification of the Choleski method of matrix inversion [33, p. 191] was programmed using the S.O.A.P. II procedure [34].

(a) Steady State Solution

To find the initial steady state solution Δt was set equal to infinity i.e. $\phi = O$ in (14), and the set of six simultaneous equations of the form

$$X_{m-1} - \left(1 + \frac{Ga}{L}\right) X_m + \frac{Ga}{L} X_{m+1} = O \quad \ldots\ldots (19)$$

was solved for the six unknown concentrations differing by at most one in the fourth decimal place from the values in Table 2.

TABLE 5
ONE TIME INTERVAL*

	R_x (ohms)	928	789	670	569	484	411	349
	R_o (ohms)	—	5000	4248	3610	3066	2605	2214	—
	Stage No.	O	1	2	3	4	5	6	7
	Initial Steady State	O	.123	.227	.315	.391	.455	.509	.556
1	Expected	O	.144	.269	.382	.489	.595	.707	.833
	Measured	B.C.	.144	.269	.381	.488	.592	.705	B.C.
	Difference		0	0	−.001	−.001	−.003	−.002	

TABLE 6
TWO TIME INTERVALS*

	R_x (ohms)	1856	1577	1340	1138	967	822	698
	R_o (ohms)	—	5000	4248	3610	3066	2605	2214	—
	Stage No.	O	1	2	3	4	5	6	7
	Initial Steady State	O	.123	.227	.315	.391	.455	.509	.556
1	Expected	O	.132	.248	.352	.452	.557	.677	.833
	Measured	B.C.	.133	.247	.352	.452	.554	.675	B.C.
	Difference		.001	−.001	0	0	−.003	−.002	
2	Expected	O	.146	.274	.391	.502	.612	.724	.833
	Measured	B.C.	.146	.274	.390	.501	.611	.722	B.C.
	Difference		0	0	−.001	−.001	−.001	−.002	

*Values of the voltages are greater than the values of the corresponding concentrations by a factor of two.

Since there is no truncation error involved in Equation (19), it is an exact expression.

The same method may be used for the final steady state.

(*b*) *Transient Solution*

The computer program was arranged so that the concentrations on each tray were calculated from time zero, when the step change in inlet gas concentration occurred, until one hour after the change, when the concentrations were easily within one per cent of steady state. Time intervals from 0.25 minutes to 60 minutes were used.

Table 7 presents the results at $t = 10$ minutes on each tray. These values are used to draw the continuous lines in Figure 5, on example of h^2-extrapolation (35). An analytical value was available for tray 6 from Acrivos and Amundson's work, and it is apparent that h^2-extrapolation is effective in this case, using either the analog results or the exact numerical solution.

Table 8 is an alternative presentation of the digital computer results, and these results show that for a finite time interval of 0.25 minutes, the numerical computation is within one per cent of the analytical values for tray 6. Figure 6 is a plot of these data together with the results of the digital computer computation for a finite time interval of five minutes.

Discussion

A severe criticism of the Liebmann analog as presently constructed was the time required for the solution of a problem. While it was very much faster than any manual numerical method

TABLE 7
APPROACH TO STEADY STATE, t = 10 MINUTES

Δt mins.	tray 1	tray 2	tray 3	tray 4	tray 5	tray 6
10	.07186	.1346	.1911	.2444	.2974	.3535
5	.07284	.1368	.1953	.2511	.3063	.3620
2.5	.07354	.1385	.1984	.2556	.3117	.3661
1.0	.07414	.1399	.2008	.2589	.3151	.3683
0.5	.07441	.1405	.2017	.2601	.3162	.3690
0.25	.07456	.1408	.2023	.2608	.3168	.3693

TABLE 8
APPROACH TO STEADY STATE: BOTTOM TRAY

Time mins.	Lapidus & Amundson	t = 0.25 min.
0	.2547	.2547
1	.3087	.3056
3	.3443	.3417
5	.3562	.3554
10	.3697	.3693
15	.3754	.3752
20	.3785	.3783
30	—	.3809
∞	.3821	.3820

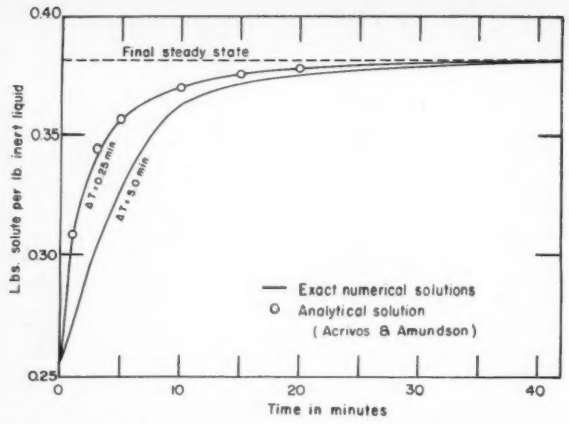

Figure 6—Rate of approach to steady state of liquid leaving the bottom tray.

of a similar accuracy, it was no faster than programming a digital computer to carry out the computation. The British Admiralty has had a Liebmann analog constructed in which potentiometers are balanced by servo mechanisms [36]. This modification would speed the solution enormously.

A second criticism is the fact that this analog cannot be used in the investigation of control dynamics. If an analog of the Paschkis type had been used, the truncation errors would vanish for the solution of the problem on gas absorption in a stagewise process and the solution would proceed automatically, thereby being extremely useful for investigating control dynamics. However, the cost of the Paschkis type of equipment would be far greater and the experimental troubles of greater complexity, particularly the introduction of non-linearities as the solution proceeds. Non-linearities should be easily introduced on the Liebmann analog, for example by varying α in Equations (13) or (14) with concentration; however, the authors have not investigated this modification extensively.

It is suggested by this work that the use of forward finite differences to approximately represent a time derivative might be discontinued in favor of either backward differences following Liebmann's work, or by using the method of Crank and Nicolson. Perhaps the backward differences are simplest when a digital computer is available.

Nomenclature

A_m = composition of liquid on the n *th* plate at time $t = O$; lb. solute 1 lb. inert absorbent
C = capacitance; farads
C' = concentration of diffusing material
$f(t)$ = boundary condition of liquid flowing to the top plate; a function of time
$g(t)$ = boundary condition of gas flowing to the bottom plate; a function of time
G = inert gas rate; lb./hr. (solute free)
H = vapor hold-up; lb. of inert gas
h = liquid hold-up; lb. of inert liquid
I = electric current; amperes
L = absorbent rate; lb./hr. (solvent free)
m = stage number
M = total number of stages
n = time interval number
R = resistance; ohms/unit length
R_{Om} = series resistor; ohms
R_m = network resistor; ohms
T = dimensionless time
t = time; hours or minutes
V = electric potential; volts
X_m = concentration of liquid leaving the m *th* plate; lb. solute/lb. inert absorbent
x = space variable; length
x' = dimensionless space variable
Y_m = composition of vapor leaving the n *th* plate; lb. solute inert gas
α = vapor liquid equilibrium constant
β = vapor liquid equilibrium constant
Δ = finite difference operator

$$\theta = \frac{G\alpha}{L}$$

$$\phi = \frac{H\alpha - h}{L\Delta t}$$

References

(1) Williams, T. J., Petroleum Refiner, **35,** No. 4, 211 (1956).
(2) Liebmann, G., Trans. A.S.M.E., 655 (1956).
(3) Bardeen, J., Phys. Rev. **57,** 35 (1940).
(4) Cohen, K., J. Chem. Phys. **8,** 588 (1941).
(5) Colburn, A. P. and Stearns, R. F., Trans. A.I.Ch.E. **37,** 291 (1941).
(6) Rose, A. and Welshans, L. M., Ind. Eng. Chem. **32,** 668 (1940).
(7) Smoker, E. H. and Rose, A., Trans. A.I.Ch.E. **36,** 285 and 675 (1940).
(8) Marshall, W. R. and Pigford, R. L., "The Applications of Differential Equations to Chemical Engineering Problems" (University of Delaware, 1947).
(9) Lapidus, L. and Amundson, N. R., Ind. Eng. Chem. **42,** 1071 (1950).
(10) Pigford, R. L., Tepe, J. B. and Garrahan, C. J., Ind. Eng. Chem. **43,** 2592 (1951).
(11) Rose, A. et al., Chem. Eng. Prog. **49,** 15 (1953).
(12) Rose, A. and Williams, T. J., Ind. Eng. Chem. **42,** 2145 and 2494 (1950).
(13) Acrivos, A. and Amundson, N. R., Ind. Eng. Chem. **45,** 467 (1953).
(14) Acrivos, A. and Amundson, N. R., Ind. Eng. Chem. **47,** 1533 (1955).
(15) Rose, A. and Williams, T. J., Ind. Eng. Chem. **47,** 2284 (1955).
(16) Rose, A. et al., Ind. Eng. Chem. **48,** 1173 (1956).
(17) Jackson, R. F. and Pigford, R. L., Ind. Eng. Chem. **48,** 1020 (1956).
(18) Mickley, H. S., Sherwood, T. K. and Reed, C. E., "Applied Mathematics in Chemical Engineering", (2nd Ed., McGraw-Hill, 1957).
(19) Rosenbrock, H. H., Trans. Inst. Chem. Engrs. **35,** 347 (1957).
(20) Crank, J. and Nicolson, P., Proc. Camb. Phil. Soc. **43,** 50 (1947).
(21) Rose, A., Sweeney, R. F. and Schrodt, V. N., Ind. Eng. Chem. **50,** 737 (1958).
(22) Hartree, D. R., "Calculating Instruments and Machines", University of Illinois Press, Urbana (1949), Chapter 3.
(23) Karplus, W. J., "Analog Simulation", McGraw-Hill (1958).
(24) Beuken, C. L., Economish Technish Tijdschrift, no. 1 (1937).
(25) Sokoln'koff, I. S. and Redheffer, R. M., "Mathematics of Physics and Engineering", McGraw-Hill (1958).
(26) Paschkis, V. and Baker, H. D., Trans. A.S.M.E. **64,** 105 (1942).
(27) Paschkis, V. and Hlinka, J. W., Trans. New York Acad. Sciences, Ser. II, **19,** 714 (1957).
(28) Liebmann, G., Brit. J. Appl. Phys. **6,** 129 (1956).
(29) Crank, J., "Mathematics of Diffusion", Oxford (1956).
(30) Courant, R., Freidrichs, K. and Lewy, H., Math. Ann. **100,** 32 (1928).
(31) O'Brien, G. G., Hyman, M. R. and Kaplan, S., J. Math. Phys. **29,** 223 (1951).
(32) Yesberg, D., M.A.Sc. Thesis, University of Toronto (1959).
(33) Hartree, D. R., "Numerical Analysis", 2nd Ed., Oxford (1958).
(34) Soap II Programmer's Reference Manual, IBM Corp., New York (1957).
(35) Richardson, L. F., Phil. Trnas. R. Soc. Lond. **226A,** 299 (1927).
(36) Sunvic Controls Ltd., "Resistance Network Analogue Computer", (Descriptive Pamphlet).

★ ★ ★

Preparation of Aluminum Octanoate and Aluminum Isooctanoate[1]

J. A. WHEAT[2], D. A. MacLEOD[2], R. G. DUNLOP[2], and H. SHEFFER[2]

Two aluminum soaps have been prepared as hydrocarbon gelling agents. The aluminum soap of 2-ethylhexanoic acid (Octal) was successfully prepared by a pilot plant continuous process which utilized a flash mixer. Optimum process conditions and the effect of important process variables were determined. There was a seasonal cycle of short gelling times and low gel consistencies in the summer months and high results in the winter. The cause of the cycle is not known.

Aluminum isooctanoate (Isooctal) was prepared continuously and batchwise on both a laboratory and pilot plant scale. The continuously prepared products were not satisfactory. Good Isooctals were prepared batchwise and pilot plant results were the same as those obtained in the laboratory. Gel consistencies showed a seasonal cycle but thickening rates did not.

ALUMINUM soaps have been widely used to thicken hydrocarbon solvents in the manufacture of lubricating greases, paints, inks, and cosmetics. During World War II their use was extended to the thickening of gasoline for incendiary bombs and flame throwers. This paper describes some of the work done in these laboratories on methods of preparation of aluminum soaps for this latter purpose.

Aluminum soaps for thickening hydrocarbon solvents are prepared by combining in aqueous solution the fatty acid, alkali, and an aluminum salt. They consist mainly of aluminum hydroxy disoap but also contain small quantities of aluminum dihydroxy monosoap, free fatty acid, and aluminum hydroxide [1, 2, 3, 4]. Aluminum trisoaps have been prepared [3, 4] under anhydrous conditions but are not formed in aqueous solutions nor can they exist in the presence of water. The overall equation of the formation of an aluminum disoap is

$$Al_2(SO_4)_3 + 4RCOONa + 2NaOH \rightarrow 2Al(OH)(OOCR)_2 + 3Na_2SO_4$$

The reaction mechanisms have been studied [5] but will not be discussed here. The theoretical alkali requirement for disoap formation is seen to be 50% in excess of that required to convert the fatty acid to the sodium soap. This excess alkali is usually sodium hydroxide but sodium carbonate has been used in the preparation of aluminum stearate [6]. Aluminum sulphate is the most commonly enjoyed aluminum salt but the chloride can also be used [7].

[1]*Manuscript received October 19, 1959; Accepted January 18, 1960*
[2]*Defence Research Chemical Laboratories, Ottawa, Ont.*
Contribution from Defence Research Chemical Laboratories, Ottawa, Ont.
Issued as D.R.C.L. Report No. 305.

In the simplest batch production method, a solution of aluminum sulphate (alum) is added to a sodium soap solution containing the excess sodium hydroxide, or the alkali-sodium soap solution can be added to the alum. Another variation is to add the alum and excess alkali simultaneously to a sodium soap solution. In general, there are a number of additional ways in which three reactants can be combined either simultaneously or in sequence but in this particular case most of them cannot be used because mixing the alum and excess alkali would produce insoluble aluminum hydroxide.

To combine liquids continuously, equipment may range from flash mixers such as a spinning disc or a centrifugal pump to stirred tanks either singly or in series [8]. Stirred tanks may follow flash mixers to give increased retention time or to serve as surge tanks; they may be operated continuously or batchwise. Woods and Taylor [4] developed a multiple stirred tank system for aluminum soaps and a British patent [9] describes a similar system but with the alum added in two stages and the excess alkali added to a third vessel. In these laboratories, continuous methods based only on flash mixing devices were investigated. The essential difference between any continuous process and the simple batch process is that in the former all the product is formed at a single pH level while in the latter the pH changes from about 12.5 to 3.5-4.5. A continuous process based on a flash mixer differs from stirred tank continuous processes as well as batch processes in that *the product is quickly withdrawn from the reaction zone and not allowed to contact unreacted chemicals.* More reproductible products would therefore be expected from the flash reactor system.

The product is separated from the mother liquor by filtering or centrifuging and, after washing with water, is dried and ground. Most soaps are easily filtered or centrifuged but washing is quite slow because sulphate is strongly held by the soap. Prolonged washing is detrimental because hydrolysis is likely to occur. It is important that the wet material be comminuted before drying. It is generally believed that drying is a critical step and high speed, low temperature drying as in a flash dryer is favored but rotary [10] and tray dryers can be used.

Gasoline is thickened by mixing with it the desired amount of aluminum soap; with some soaps heating is necessary and frequently a peptizer is added. The peptizer increases the rate of gel formation but also increases the rate of deterioration of the gel. Some peptizing action is obtained from residual water and free fatty acid but this is usually not sufficient. The more common peptizers include alcohols, Cellosolves, phenol, cresols, xylenols,

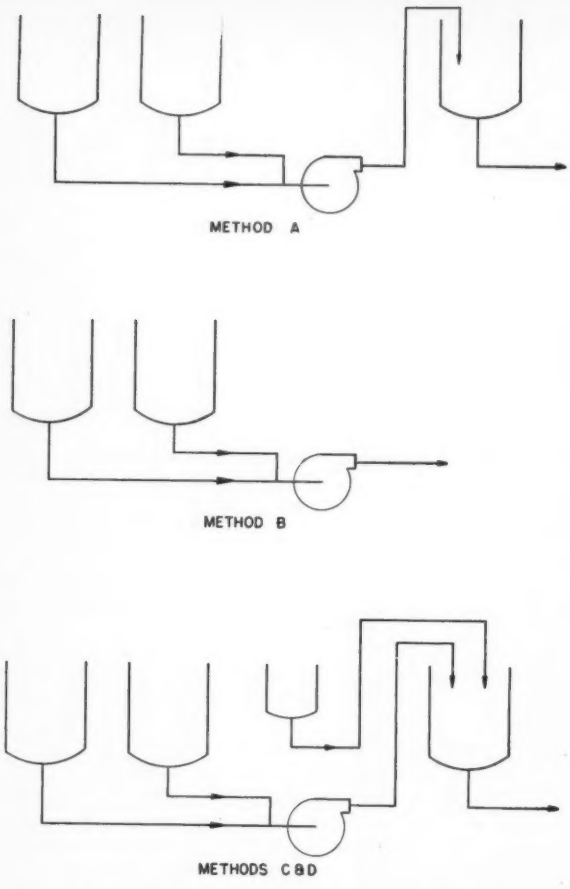

Figure 1—Continuous processes used to prepare aluminum soaps on a pilot plant scale.

and fatty acids [4, 7, 11]. The polymeric structure and properties of the gels are described in a number of papers, for example [3, 4, 7, 11, 12].

An ideal aluminum soap for thickening gasoline would have the following properties: It would readily dissolve in gasoline and rapidly form a gel over a wide range of temperatures with a minimum of stirring; A low concentration would give a high viscosity; The soap and gels prepared from it would be stable for long periods of time under a wide range of temperature and humidity conditions; The soaps and gels would be reproducible; and the soap would have a high bulk density.

It has been well demonstrated [11, 13] that aluminum soap-gasoline gels possess properties that make them good incendiary fuels but this aspect was not considered in the work being reported here. All soaps were compared on the basis of laboratory tests only.

The first aluminum soaps used extensively to thicken gasoline for fire bombs and flamethrowers were aluminum stearate [11] in the United Kingdom and Napalm [10, 13, 14] in the United States. Napalm was made by coprecipitating a mixture of naphthenic acids, oleic acid, and the acids from coconut oil. The principal constituent of coconut oil is lauric acid and this led to the study of aluminum laurate [4, 9]. A number of other fatty acids such as mixed isooctanoic acids [15] and 3,5,5-trimethylhexanoic acid [16] have been investigated. In these laboratories, experimental work was concerned largely with four acids, 2-ethylhexanoic acid, mixed isooctanoic acids prepared by an oxo [17] process, stearic acid, and lauric acid. Data for the first two of these are reported in this paper.

EXPERIMENTAL

Soaps were prepared batchwise and continuously on both a laboratory and pilot plant scale. Most of the work, however, was done on a pilot plant scale. The laboratory processes were introduced because supplies of isooctanoic acid were limited.

Figure 1 illustrates the four continuous or semi-continuous processing methods used. In Method A, sodium soap plus excess sodium hydroxide was combined with alum solution and the resulting slurry held for a time in a tank before centrifuging. In Method B, the slurry was sent directly to the centrifuge. In the other two methods, sodium soap and alum solution were combined in a flash mixer; in Method C excess alkali was added simultaneously to the slurry tank while in Method D the alkali was added batchwise after stopping the flow of the other two solutions.

Pilot Plant Equipment

For pilot plant continuous runs 10 lb. of fatty acid and the desired amount of sodium hydroxide were dissolved in water in one of the solution tanks shown in Figure 2 to give 22 gal. of solution. Alum solution was prepared in the other tank so that an equal volume gave 5-10% excess alum. These solutions were pumped at equal rates of about 0.75 g.p.m. by the two halves of a duplex reciprocating pump. The pulsations in the discharge were smoothed out by a system of orifices and surge tanks. An orifice diameter of about 1/16 in. was used and the surge tanks were 3 in. in diameter by 15 in. long. The back pressure built up to 20-30 p.s.i. gauge and fluctuated only 2-3 p.s.i. over the suction-discharge cycle of the pumps so the liquid flow from each orifice was essentially smooth and uniform. When excess alkali was added separately it was pumped with both halves of a second duplex reciprocating pump with a total capacity of 4.9 g.p.h. Pulsations in the flow of this third solution were not detrimental. The alum and sodium soap solutions were led by means of concentric pipes to the inside of either a colloid mill or a centrifugal pump. The colloid mill, which was used first, had a 3 in. diameter rotor driven at 7300 r.p.m. Since it was usually operated at maximum clearance of 0.05 in. any spinning disc would probably have worked as well. The centrifugal pump had an open 6 in. impeller and a speed of 3450 r.p.m. Both units had 3 h.p. motors. The flow of solutions was stopped after 24 min. and the remaining processing steps carried out batchwise.

Slurry was transferred to a centrifuge using a centrifugal pump and the product collected in a 26 in. diameter basket operated at 855 r.p.m. It was washed at 1-2 g.p.m. for about 20 min. and then spun for 5-10 min. at 1710 r.p.m. It was then removed with an unloading blade, spread 0.1-0.5 in. deep on screen bottom trays 18 x 28 x 2 in. deep, and placed in a tray dryer. The dry bulb temperature of the dryer was automatically controlled by regulating the flow of steam to a heater and the wet bulb temperature by regulating a steam spray. The air velocity was about 250 ft./min. A constant drying time of 21 hr. was used and, except for special tests, Octal was dried at 60°C. and Isooctal at 78°C. A higher temperature was needed for drying Isooctal not to increase the rate of drying but because Isooctal had a higher equilibrium moisture content. Dried soap was removed from the dryer and ground in a 6. in. hammer mill.

The same equipment was used for batch precipitation by preparing the sodium soap solution in the slurry tank

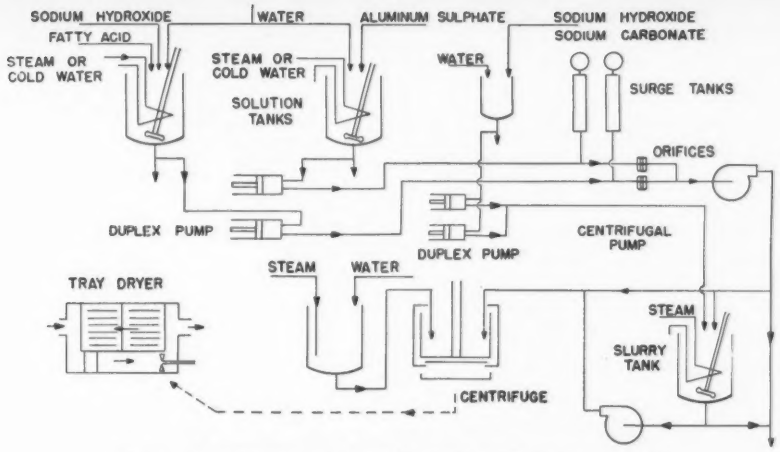

Figure 2 — Diagram of pilot plant equipment used to prepare aluminum soaps.

and adding a relatively concentrated alum solution via the excess alkali system over a period of about 18 min.

All equipment and piping except the copper wash water tank were 304 or 316 stainless steel.

Laboratory Apparatus

Batch and continuous laboratory runs were made with 50 g. of fatty acid in 500, 1000, or 2000 ml. of solution and with a reaction time of 18-20 min. In batch operation the reactants were mixed in a beaker by a 2 in. propeller with a variable speed drive. The rate of flow of alum solution was set by a constriction which controlled the admission of air into a separatory funnel. The product was recovered in a variable speed, 5 in. centrifuge and dried on 8 x 8 x ½ in. trays in the pilot plant dryer or a small electrically heated dryer.

In continuous operation only Method B was used with the reactants being mixed in a small centrifugal pump. At first, flow rates of the solutions were regulated with needle valves and measured with calibrated rotameters but a peristaltic action pump (Sigmamotor, Inc. Model T-63) installed later was better.

Materials

Technical grade 2-ethylhexanoic acid and mixed isooctanoic acids were purchased in 400 lb. drums from Carbide Chemicals Company, Montreal but were produced in the United States. The isooctanoic acid was the oxidized product of an oxo process [17] and the following data were supplied.

Sp. gr. 20/20°C.	0.9171
Distillation at 760 mm.	
Initial b.p.	229.0°C.
50%	231.7°C.
End point	239.2°C.
Purity	96.9%
Water	0.04%
Ester	0.08%
Odor	70°

Flake caustic soda was purchased in 380-400 lb. drums and commercial grade, iron free aluminum sulphate ($Al_2(SO_4)_3 \cdot 18H_2O$) was purchased in 100 lb. bags.

Test Methods

Octal gels were prepared by dispersing 1.5% Octal in gasoline with 0.5% distilled 2-ethylhexanoic acid as peptizer. Isooctal was tested at a concentration of 2% with no peptizer. The time for the vortex to disappear when mixing the ingredients under standard conditions was reported as stir time. Gel consistency was measured with a Gardner mobilometer and the results were reported as the weight required to give a constant rate of shear. Gels were tested first after two days and then each succeeding week from the date of preparation. These later results were reported as a percentage of the 2-day value. Ordinary leaded gasoline was used for all gel tests. When replacement was necessary, samples of gasoline were obtained from Ottawa distributors and compared against a standard lot of Octal. A drum of the gasoline most closely resembling the previous drum was purchased.

The moisture content of both wet and dry soap was determined with an infra-red moisture balance (Central Scientific Company, Chicago) with a 125 watt infra-red lamp mounted about 1.5 in. from the sample. Octal samples were left on the balance until they reached constant weight. For wet material, 30-40 min. was required while for dried product, 10 min. was sufficient. Isooctal samples decomposed if left too long and it was necessary to plot loss in weight against time and take the first abrupt change in slope as the moisture content. This change in slope was usually readily detected. All moistures were reported on the wet basis.

Bulk density was determined by measuring the volume of about 35 g. of dry product in a 250 ml. graduate. The cylinder was tapped on the bench top either manually or mechanically to obtain a minimum volume.

RESULTS — OCTAL

Seasonal Variation

Throughout the work on this project there were several unaccounted for changes in stir time and Gardner consistency. Since these appeared to be related to time of production, graphs were prepared of weekly average results plotted against numbers representing the weeks of the year. Figures 3 and 4 show the changes of weekly stir time and 2-day Gardner consistency with date of preparation for all lots of Octal that could be reasonably included in the averages. The same data are presented in Figures 5 and 6 after smoothing by means of a seven-point moving average. These graphs show a definite seasonal cycle that is remarkably reproducible from one year to the next.

Several samples of Octal were tested over a period of time and, as shown in Table 1, these results followed the same seasonal trend as freshly produced samples. How-

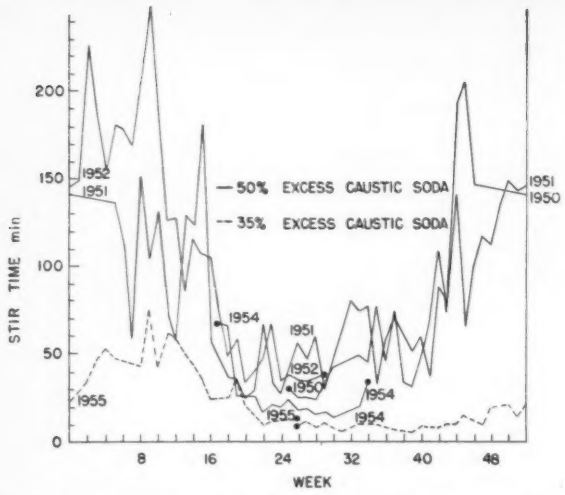

Figure 3—Variation of weekly average stir time of Octal gels with date of preparation.

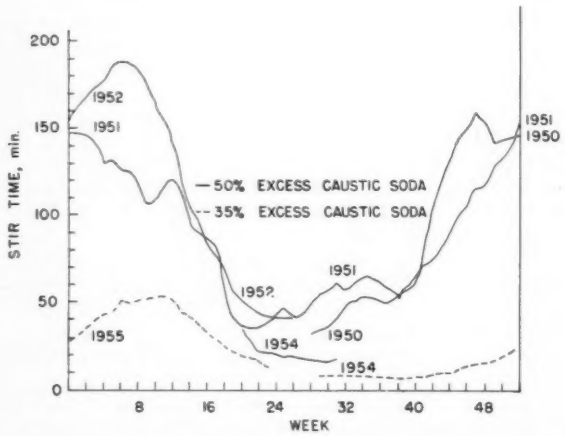

Figure 5—Lines of Figure 3 after smoothing by plotting a moving seven point average.

ever, when winter and summer soaps were tested at the same time, the winter soaps did give higher results than the summer soaps. Thus, the test results depended upon both time of production and time of testing. Weekly average results of 1954-1955 (Figures 3 and 4) were compared with weekly averages of daily mean temperature and daily mean absolute humidity. As expected, the general trend of the curves were in agreement, however weekly fluctuations in test results did not correspond with weekly fluctuations in temperature or humidity.

TABLE 1
EFFECT OF TIME OF TEST FOR TWO GROUPS OF OCTALS PREPARED WITH 35% EXCESS SODIUM HYDROXIDE

Week of test	Stir time, min.	2-day Gardner consistency, g.
1 Nov. 1954*	10	186
17 Jan. 1955	21	176
21 Feb. 1955	21	187
28 Mar. 1955	34	184
6 Jun. 1955	8	139
28 Feb. 1955*	68	213
13 Jun. 1955	14	125

*Time of Production

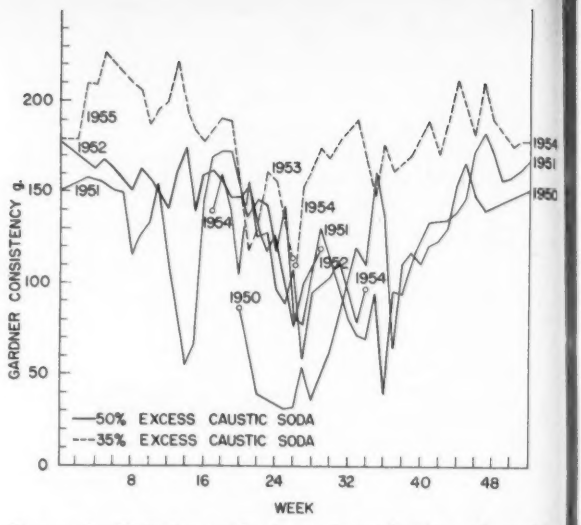

Figure 4—Variation with date of production of weekly average 2-day Gardner consistency of Octal gels.

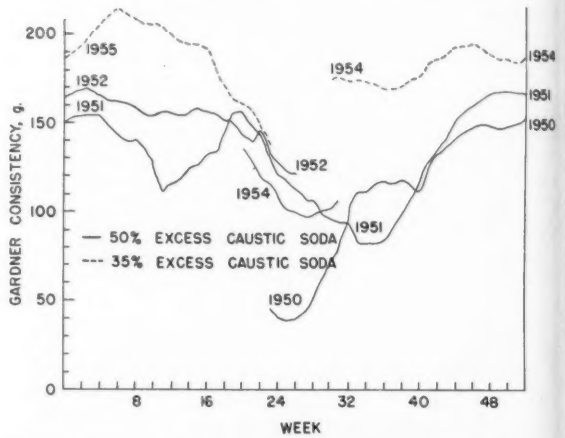

Figure 6—Lines of Figure 4 after smoothing by plotting a moving seven-point average.

The direct cause of the seasonal cyle is not known but its presence had to be taken into account in planning experiments and interpreting results. In all experiments, adequate controls were included and results compared with these controls rather than previous data. Factorial experiments, which sometimes took from three to six weeks to complete, were carried out in randomized blocks and nearly always there was a statistically significant block effect in accord with the seasonal cycle.

Preparation of Solutions

The effect of excess sodium hydroxide on both summer and winter soaps is shown in Table 2. As the amount was reduced from the theoretically required 50%, the stir time became shorter and initial gel strength higher but the gels tended to be less stable. Figures 5 and 6 also show that 35% excess alkali gave lower stir times and higher gel consistencies than 50%. A level of 35%, which was selected as optimum, had the disadvantage that the product yield was about 75% of theoretical as compared with 80% when 50% excess sodium hydroxide was used. All yields were low probably because of incomplete reaction or hydrolysis during washing since mechanical losses were not large.

TABLE 2

EFFECT OF SOLUTION VARIABLES ON GEL FORMING PROPERTIES OF OCTAL

Temp., °C.	Soln. concn., lb. acid/gal.	Excess sodium hydroxide, %	Number of runs	Stir time, min.	2 day Gardner consistency, g.	Stability, %	
						7 days	21 days
40	0.45	30	12	7	170	47	24
40	0.45	35	12	8	170	54	24
40	0.45	40	12	12	160	66	30
40	0.45	50	12	17	100	82	52
40		30	8	46	200	85	28
40		35	8	64	206	78	36
40		40	8	71	177	87	51
40		50	8	87	128	70	31
40	0.23	30	12	17	201	74	32
40	0.45	30	12	11	193	71	24
40	0.91	30	12	10	191	64	26
40	0.45	35	4	73	203	80	33
40	0.91	35	4	54	208	82	40
25	0.45	35	6	9	169	57	22
40	0.45	35	6	9	158	54	25
70	0.45	35	6	14	158	61	—

Increasing the level of excess alum from 10% to 30% had no effect. This means that relative pumping rates of the two solutions could vary over a wide range without affecting the product.

As the reactant solutions were concentrated, stir time decreased markedly (Table 2) but gel consistencies were not affected. Thus, concentrated solutions are preferable. This is an economic advantage as well. For most of the experimental work however, the intermediate concentration of 0.45 lb. of acid/gal. was used because this concentration gave the same results as 0.91 lb./gal. but the consumption of chemicals was lower.

There was no difference between reaction temperatures of 25 and 40°C. but at 70°C. the stir time was higher (Table 2). With 50% excess sodium hydroxide, the temperature effect was greatly magnified and soaps prepared at 70°C. had very long stir times and gave very weak gels.

Reaction Conditions

There was no difference between Octals prepared with the colloid mill and those prepared with the centrifugal pump. A centrifugal pump would be preferred because it has a lower first cost. Reducing the flow rates by one-half did not improve the product so the higher rate is preferable. Data on the effect of mature time and a three solution method of preparation are given in Table 3. It is apparent that the three solutions method gave an inferior product and that 60 minutes mature time was neither necessary nor detrimental.

TABLE 3

EFFECT OF MATURE TIME AND PREPARATION METHOD (OCTAL)

Production method	Retention time, min.	Number of runs	Stir time, min.	2 day Gardner consistency, g.	Stability, %	
					7 days	21 days
A	0	6	11	192	67	25
A	60	6	12	194	74	25
A	0	12	37	198	69	19
B	—	12	40	198	72	19
A	0	4	49	209	99	62
C	0	4	63	140	36	—

Centrifuging and Drying

With the standard 10 lb. of acid per run, the centrifuge cake was about 1 in. thick and had a moisture content of 55%. With only 5 lb. of acid the moisture content was 65% and when 20 lb. of acid was used it was 45%. In two special runs the centrifuge basket was filled to the maximum thickness of 3.5 in. with no detectable decrease in filtration or washing rate. The average moisture content was about 40%.

The effect of final moisture content on the gelling properties of Octal is shown in the first portion of Table 4. These data were obtained by drying trays with different amounts of Octal for a uniform time of 21 hr. Using an average slope, it was calculated that increasing the moisture content from 1% to 2% reduced the stir time 2.7 min. and the 2-day Gardner consistency only 14 g. Even at almost 4% moisture, the gel consistency was still 158 g.

The second portion of Table 4 shows the effect of dryer temperature. The tray loading was also varied in order to obtain a more nearly constant final moisture content. Under these conditions dryer temperature from 60 to 80°C. had little effect. At 90°C. gel consistencies were lower and at 50°C. stir time and gel stability were lower. Some Octals were freeze dried at a maximum temperature of 24°C. and the average stir time was about

TABLE 4

EFFECT OF DRYING CONDITIONS ON GELLING PROPERTIES OF OCTAL

Dryer temp., °C.	Tray loading, lb./sq. ft.	Moisture, %	Stir time, min.	2 day Gardner consistency g.	21 day stability, %
60	0.4	0.8	13	210	20
60	0.5	1.1	12	182	21
60	0.5	1.7	11	188	24
60	0.9	2.6	9	174	24
60	1.2	3.2	7	173	24
60	1.4	3.9	6	158	25
50	0.6	2.0	16	191	19
60	0.9	1.4	28	177	37
70	1.1	1.1	27	161	38
80	1.2	1.1	42	178	48
90	1.6	1.4	28	110	31

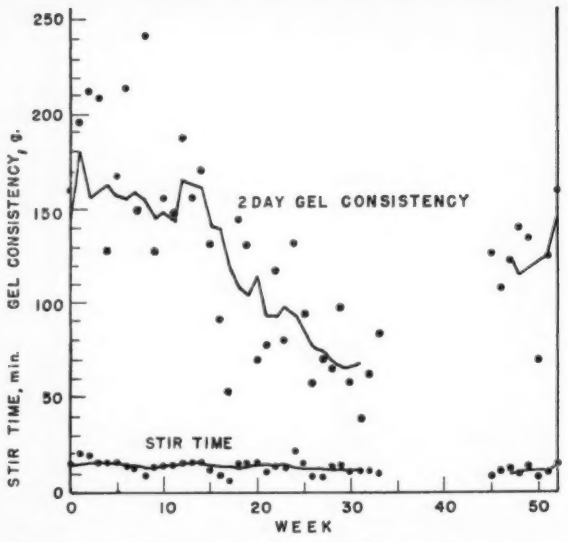

Figure 7—Effect of date of production on properties of gels of Isooctal prepared batchwise on a laboratory scale.

one-half that of material tray dried at 60°C. The initial gel consistencies were the same but gels of the freeze dried product were less stable.

Excellent results were obtained when Octal was flash dried in a No. 40 Raymond Imp Mill Flash Dryer at Mallinckrodt Chemical Works Limited, Montreal. Gel consistencies were the same as those of tray dried Octals but stir times were reduced to about one-third, although this may have been largely because the tray dried material was not ground. These data cannot be compared with the results obtained here because the soaps were prepared batchwise. Nevertheless, flash drying would be an ideal method for large scale continuous processing.

Miscellaneous

The average bulk density of Octal was about 0.20 g./ml. and on a Tyler "Rotap" apparatus 98% passed 100 mesh and 13% passed 200 mesh.

Summary

The optimum or standard conditions for preparing Octal by the pilot plant continuous process were as follows:

Sodium soap solution concentration	4.5% acid (0.45 lb./gal.)
Excess sodium hydroxide	35%
Excess alum	10%
Reaction temperature	40°C.
Pumping rate	0.750 g.p.m.
Wash water	35 lb./lb. acid
Drying temperature	60°C.
Drying time	21 hr.
Tray loading	0.5 lb./sq. ft.
Final moisture content	0.6-1.2%

RESULTS — ISOOCTAL

Production by Continuous Process

All Isooctals prepared continuously were very poor. The average stir time for 65 laboratory runs using Method B was 32 min. and the average 2-day Gardner consistency was 36 g. The averages for 38 pilot plant runs using Method A with a mature time of 5 or 10 min. were 100 min. and 75 g. Excess sodium hydroxide was varied from 35 to 50%, reaction temperature was tested over the range from 30 to 45°C., pumping rates and solution concentrations were changed, and drying temperature was reduced from 78 to 60°C. without improvement. Nor were the results improved by the addition of acetic acid to the sodium soap solution [4, 6] or of 2% silical gel to the dried product.

Production by Batch Process

As with Octal, 2-day Gardner consistency results showed a pronounced seasonal cycle but the stir time cycle, if present at all, was very small. The points in Figure 7 are weekly average stir times and 2-day Gardner consistencies while the lines were drawn through moving five-point averages with the weekly averages weighted according to the number of runs available. Only the results for laboratory soaps prepared under standard conditions were used. These standard conditions were as follows:

Sodium soap solution concentration	5% acid
Excess sodium hydroxide	40%
Alum solution concentration	40%
Excess alum	5%
Reaction temperature	40°C.
Reaction time	18 min.
Mature time	10 min.
Wash water	40 g./g. acid
Drying temperature	78°C.
Drying time	21 hr.
Tray loading (laboratory	0.25 lb./sq. ft.
(pilot plant)	0.7 lb. /sq. ft.
Final moisture content	0.6-1.2%

As seen in Figure 7, stir times were 10-15 min. and 2-day Gardner consistencies varied from 70 g. in the summer to 155 g. in the winter. Gel stabilities were about 42% at 7 days and 20% at 28 days.

TABLE 5
EFFECT OF PROCESS VARIABLES ON GEL FORMING PROPERTIES OF ISOOCTAL

Excess sodium hydroxide, %	Reaction temp., °C.	Reaction time, min.	Wash water, g./g/ acid	Stir time, min.	2 day Gardner consistency, g.	28 day stability, %
35	40	18	40	11	113	21
40	40	18	40	13	118	25
45	40	18	40	15	144	19
50	40	18	40	16	131	22
40	30	18	40	14	131	25
40	40	18	40	13	170	15
40	50	18	40	16	183	20
40	40	9	40	12	129	18
40	40	18	40	13	170	15
40	40	36	40	18	172	31
40	40	18	20	18	81	21
40	40	18	40	20	95	25
40	40	18	80	29	100	25
40	40	18	160	30	135	30

TABLE 6
RINSING WITH CALCIUM AND BARIUM SOLUTIONS (ISOOCTAL)
(Number of runs = 4)

Rinse solution	Stir time, min.	2 day Gardner consistency, g.	28 day stability, %
None	12	138	22
$Ca(OH)_2$	6	93	38
$Ba(OH)_2$	11	134	26
$CaCl_2$	7	80	10
$BaCl_2$	9	100	22

TABLE 7

EFFECT OF ADDITIVES (ISOOCTAL)
(1% to soap solution, Number of runs = 3)

Additive	Stir time, min.	2 day Gardner consistency, g.	28 day stability, %
None	15	156	16
Tween 40	13	161	11
Ammonyx CO	10	182	10
Acacia gum	11	140	12
Acetic acid	13	215	17

Both stir time and gel consistency increased slightly with excess sodium hydroxide, reaction temperature, reaction time, and amount of wash water (Table 5) but over the range from 2.5-10 g. of acid/100 ml., sodium soap solution concentration did not affect the gel forming properties.

It was thought that sulphate remaining in the product could be precipitated with barium or calcium solutions. Thus, following the regular water wash, the centrifuge cake was rinsed with 500 ml. of solutions containing 1.5 g./liter of barium or calcium hydroxide or 15 g./liter of barium or calcium chloride. Of the four solutions tried only calcium hydroxide looked promising (Table 6). Stir time was considerably lower and stability was higher but 2-day consistency was not as high.

In an experiment on the effect of additives (Triton X-45, Tween 40, Ammonyx *CO*, acetic acid, adipic acid, gelatine, glue, locust bean gum, guar gum, acacia gum, carboxymethyl cellulose) at a level of 1% of the acid it was found that it made no difference whether materials were added to the sodium soap solution or to the alum except that a number of them were precipitated by the alum. On a large scale this precipitate would cause no difficulty but on a laboratory scale it made it impossible to add the alum solution slowly and uniformly to the soap solution. All additives tested increased gel strength and stability but nearly all of them also increased stir time. In a second experiment, four of the most promising materials were tested at levels of 0.4, 1.0, 2.0 and 5.0% of the acid. Results for the 1% level are given in Table 7. Acetic acid and Ammonyx *CO* were the best, giving slightly lower stir time and considerably higher gel consistencies.

Batches prepared on a pilot plant scale gave the same results (Table 8) as laboratory batches prepared during the same period.

DISCUSSION

Octal was successfully prepared by a pilot plant continuous process but Isooctal had to be made batchwise. However, Isooctal had a bulk density more than 2.5 times that of Octal and it could be used without a peptizer. Both stir time and Gardner consistency of Octal gels had a pronounced seasonal cycle but only the consistency of Isooctal gels changed with time of production. Because of the seasonal cycles it was not possible to estimate which acid or which process gave more uniform results.

Acknowledgement

Thanks are due to A. E. Leger and W. D. Barnes for conducting gel tests.

References

(1) Gallay, W., and Puddington, I. E., Can. J. Research, **B, 26,** 155 (1948).
(2) Coe, R. H., Mysels, K. J., and Smith, G. H., J. Colloid Sci., **3,** 293 (1948).
(3) Leger, A. E., Haines, R. L., Hubley, C. E., Hyde, J. C., and Sheffer, H., Can. J. Chem., **35,** 799 (1957).
(4) Woods, D. E., and Taylor, A. J., J. Appl. Chem., **8,** 237 (1958).
(5) Bullof, J. J., Ph.D. Thesis, Rensselaer Polytechnic (1953).
(6) Edwards, L. J., Brit. Patent. 587,522, April 29, 1947.
(7) Sheffer, H., Can. J. Research, **B, 27,** 791 (1949).
(8) Olsen, J. F., and Lyons, E. J., Chem. and Met. Eng., **52,** No. 5, 118 (1945).
(9) Wilson, E., Brit. Patent 693,741, July 8, 1953.
(10) Chemical Week, 69, Sept. 22, 26 (1951).
(11) Cawley, C. M., Carlile, J. H. G., King, J. G., and Kingman, F. E. T., J. Inst. Petroleum, **33,** 721 (1947).
(12) Leger, A. E., Hyde, J. C., and Sheffer, H., Can. J. Chem., **36,** 1584 (1958).
(13) Fieser, L. F., Harris, G. C., Hershberg, E. B., Morgana, M., Novello, F. C., and Putman, S. T., Ind. Eng. Chem., **38,** 768 (1946).
(14) Mysels, K. J., Ind. Eng. Chem., **41,** 1435 (1949).
(15) Cohen, L., U.S. Patent 2,741,629, April 10, 1956.
(16) Taylor, A. J., and Woods, D. E., J. Appl. Chem., **8,** 251 (1958).
(17) Kirk, R. F., and Othmer, D. F., Encyclopedia of Chemical Technology, Vol. 9, p. 699, Interscience Publishers Inc., New York (1952).

TABLE 8

COMPARISON OF LABORATORY AND PILOT PLANT BATCH OPERATION (ISOOCTAL)

Scale	Number of runs	Moisture, %		Bulk density, g./ml.	Stir time, min.	2 day Gardner consistency, g.	Stability, %	
		cake	dry				7 days	28 days
Laboratory	44	32.5	1.1	0.55	12	69	36	21
Pilot Plant	9	36.6	1.0	0.54	11	77	39	21

★ ★ ★

The Upward Vertical Flow of Air-Water Mixtures

III. Effect of Gas Phase Density on Flow Pattern, Holdup and Pressure Drop[1]

R. A. S. BROWN[2], *G. A. SULLIVAN*[3] *and G. W. GOVIER*[4]

Results of measurements of pressure drop and holdup are reported over a range of air and water rates for the upward vertical flow of air-water mixtures in a 1.50 inch I.D. tube with average air densities ranging from 0.092 to 0.552 lb./ft.^{3} Superficial water velocities were between 0.0695 and 7.35 ft./sec..

The data are analyzed by the method first suggested by Govier, Radford and Dunn and later used by Govier and Short. This involves the division of the flow range into four regimes on the basis of the pressure drop curves (to aid correlation of flow pattern and holdup data) and the separation of the unit pressure drop into hydrostatic and irreversible components. A superficial friction factor is calculated from the irreversible component of the unit pressure drop.

The average density of the gas phase has a more or less marked effect on all three regime transitions. The transitions all shift similarly to lower air-water discharge volume ratios with increasing gas phase density. While the flow patterns were not directly observed in the investigation here reported, the flow pattern transitions would be expected to behave similarly.

Over the range investigated, the gas phase density has little or no effect on the superficial friction factor. The holdup ratio is unaffected by the gas phase density in Regimes I and II but is significantly affected in Regimes III and IV.

This paper is the third of a series based upon an experimental study of upward vertical flow of gas-liquid mixtures. The object of the study is the development of a workable correlation for the effects on the two-phase flow of:

(a) the flow rates of the two phases;
(b) the diameter of the tube, and
(c) the physical properties of the two fluids.

The pertinent physical properties are believed to be density, viscosity and interfacial tension. The quantities which have been chosen as descriptive of the two-phase flow are:

(a) unit pressure drop (i.e. pressure drop per unit length of tube);
(b) holdup ratio (i.e. the ratio of the volume ratio of the phases in the discharge mixture to that in the flow section), and
(c) the flow pattern and its relationship to the unit pressure drop curve (i.e. the unit pressure drop versus the volume ratio of the phases in the discharge mixture).

The volume ratios referred to above are in all cases the volume ratio of the gas phase to the liquid phase.

The significance of the major variables, the thermodynamic relationships controlling the pressure drop and the relationship between the holdup ratio and the relative velocities of the phases are dealt with in detail in Part I[1] of the series.

The literature on two-phase gas-liquid flow was reviewed briefly in Part I and has been covered more thoroughly in two recent bibliographic articles[2,3]. Most of the work on the subject has been devoted to the accumulation of data and the development of practical correlations with little, if any, theoretical basis. Notable among the exceptions to this generalization is the work of Calvert and Williams[4] on annular flow. The work reported in this series was undertaken for the purpose of obtaining a comprehensive set of self consistent data covering a wide range of the variables and to serve as a basis for the better physical understanding of the flow phenomena.

The first two parts of this series have dealt, as does this, with the air-water system. Part I[1] of the series was concerned with the effect of relative flow rates in a smooth bore tube having an inside diameter of 1.025 inches. For an average test section pressure of 36.0 p.s.i.a. and an average temperature of approximately 70°F. data were reported for discharge air-water ratios ranging from 0 to 248 and water rates varying from 0.00040 to 0.0421 ft.^{3}/sec. (superficial water velocities between 0.0698 and 7.35 ft./sec.). Part II[5] presented the results obtained in a study of the effect of diameter on the flow. Measurements were made under similar temperature, pressure and flow rate conditions with three additional tubes ranging from 0.63 to 2.50 inches diameter. The work reported here is primarily concerned with the effect of gas phase density on the two-phase flow, and is from a more general study of two-fluid systems[6]. Investigations now in progress deal with the effects of viscosity and interfacial tension.

The previously reported[1,5] analysis of the flow system has shown that the overall unit pressure drop (here expressed in terms of feet of water per foot of height) may be separated into two components—that due to the hydrostatic head and that due to the irreversibilities associated with the flow. From the irreversible component of the pressure drop, a friction factor, f'_L, may be defined based upon the Fanning equation and the superficial water velocity.[1,5]

[1]*Manuscript received November 5, 1959; Accepted January 14, 1960.*
[2]*Ph.D. candidate, Department of Chemical and Petroleum Engineering, University of Alberta, Edmonton, Alta.*
[3]*Chemical Engineering Section, Canadian Industries Limited, Montreal, Que.*
[4]*Professor of Chemical Engineering, Dean of Faculty of Engineering, University of Alberta, Edmonton, Alta.*

Experimental Equipment and Procedure

The experimental equipment used to obtain the data reported here[6] was essentially the same as that used in the previous investigations of the system[1,5]. The test section was a 22.88 foot length of 1.50 inch I.D. seamless copper tubing similar to that described by Govier and Short.[5] In order to obtain sufficient variation in air pressure to give a significant gas phase density change, an additional supply was obtained by parallel connection of two 125 SCFM air compressors with a maximum pressure of 200 p.s.i.g. This permitted operation at flowing pressures to 110 p.s.i.a. Tests at 18 and 36 p.s.i.a. were made using the laboratory air supply.

The method of operation of the equipment was similar to that used previously.[6] Measurements were made at three gas phase densities with the air-water system, corresponding to mid-point pressures of 18, 72 and 110 p.s.i.a. Air-water volume ratios ranged from 0.72 to 669 for water rates from 0.000851 to 0.091 ft.³/sec. (superficial water velocities from 0.0695 to 7.35 ft./sec.). In order to simplify the analysis of the data, the tests were made at approximately the same superficial water velocities as were used previously.[1,5] As it was not practical to control the ambient temperature, some variation of flow temperature between tests was experienced, but it is not believed to be significant.

Experimental Results

The basic experimental data for the air-water system are tabulated in Table 1 (partial) for gas phase densities varying

TABLE 1 (PARTIAL)

EXPERIMENTAL DATA

TUBE DIAMETER 0.125 FT.
TEST SECTION LENGTH 22.88 FT.
TEST SECTION MID POINT PRESSURE AS INDICATED
TEST SECTION MID POINT TEMPERATURE AS INDICATED
SPECIFIC VOLUME OF LIQUID PHASE = 0.01603 FT.³/LB.
SPECIFIC VOLUME OF SATURATED GAS PHASE AS INDICATED
SUPERFICIAL WATER VELOCITIES APPROXIMATELY CONSTANT AT 0.868 FT./SEC.

1	2	3	4	5	6	7	8	9	10	11
Test Number	Test Section Mid Point Pressure Psia	Water Rate ft.³/sec.	Saturated Air Rate ft.³/sec.*	Mid Point Temperature °F	Discharge Air-Water Ratio**	Test Section Air-Water Ratio**	Specific Volume Saturated Gas Phase* ft.³/lb.	Holdup Ratio***	Pressure Drop ft. H_2O/ft.	Pressure Drop Regime
27A	18.0	0.0107	0.0765	82	7.16	2.27	11.3	3.16	.296	I
28A			0.174	80	16.3	3.18	11.3	5.12	.320	III
29A			0.155	79	14.5	2.86	11.2	5.06	.276	II
30A			0.022	80	2.06	1.76	11.3	1.17	.555	I
31A			0.0375	79	3.52	1.36	11.2	2.59	.435	I
32A			0.0519	77	4.86	1.93	11.2	2.52	.370	I
33A			0.115	76	10.8	2.70	11.2	4.00	.290	II
345S	36.0	0.0107	0.396	79	37.2	5.02	5.55	7.41	.217	III
346S			0.214	66	20.1	3.52	5.41	5.71	.281	III
350S			0.282	67	26.5	3.97	5.42	6.68	.244	III
351S			0.170	67	16.0	2.70	5.42	5.93	.320	III
352S			0.128	67	12.0	2.37	5.42	5.06	.350	III
353S			0.0898	67	8.43	2.46	5.42	3.42	.337	II
354S			0.0321	67	3.01	1.47	5.42	2.05	.377	I
355S			0.0587	67	5.51	2.04	5.42	2.70	.320	I
356S			0.0197	79	1.84	0.914	5.55	2.01	.540	I
357S			0.0493	79	4.63	1.81	5.55	2.56	.293	I
358S			0.0888	80	8.34	2.70	5.56	3.09	.335	II
359S			0.338	81	31.7	4.94	5.57	6.42	.241	III
360S			0.389	80	36.5	5.15	5.56	7.09	.232	III
121A	72.0	0.0107	0.0276	86	2.59	—	2.85	—	.417	I
122A			0.0335	85	3.14	1.49	2.85	2.11	.368	I
123A			0.0433	85	4.17	2.15	2.85	1.94	.284	I
124A			0.0553	84	5.19	2.06	2.85	2.52	.255	I
125A			0.0594	80	5.57	2.40	2.85	2.32	.265	II
126A			0.0857	80	8.07	2.15	2.85	3.73	.328	II
127A			0.114	80	10.7	2.53	2.85	4.23	.309	III
128A			0.159	81	14.9	3.17	2.85	4.70	.265	III
129A			0.245	86	23.0	4.47	2.85	5.17	.235	III
130A			0.330	86	31.0	5.84	2.85	5.33	.226	III
131A			0.356	89	33.6	7.18	2.90	4.70	.278	IV
186A	110.0	0.0107	0.0215	77	2.02	1.07	1.80	1.88	.530	I
187A			0.0319	76	2.99	1.47	1.80	2.02	.392	I
188A			0.0404	80	3.79	1.58	1.80	2.40	.318	I
189A			0.0525	83	4.92	2.22	1.80	2.22	.284	II
190A			0.0615	82	5.77	2.13	1.80	2.71	.308	II
191A			0.0784	90	7.36	1.85	1.80	3.98	.352	II
192A			0.0937	95	8.81	2.02	1.80	4.36	.343	III
193A			0.1425	87	13.4	2.84	1.80	4.72	.298	III
194A			0.182	83	17.1	3.64	1.80	4.70	.265	III
195A			0.216	90	20.3	—	1.85	—	.245	III

* At test section temperature and average pressure.
** Column 4 divided by column 3.
*** Column 6 divided by column 7.

from 0.092 to 0.552 lb./ft.^{3} and for a water rate of 0.0107 ft.^{3}/sec. corresponding to a superficial water velocity of 0.868 ft./sec. The complete tabular data for the same gas phase densities and for water rates ranging from 0.000851 to 0.091 ft.^{3}/sec. are given in Table 1 deposited as Document No. 6163 with the American Documentation Institute Auxiliary Publication Project, Photo Duplication Service, Library of Congress, Washington 25, D.C.

Referring to Table 1 (partial), column 2 gives the mid-point pressure, column 3 gives the water rate in cu. ft./sec. and column 4 gives the calculated flow rate of water-saturated air at mid-point conditions. The mid-point temperature is given in column 5. The quotient of column 4 and column 3, the volume ratio of the air to water rates is given in column 6, while the volume ratio of air to water in the test section is given in column 7. The specific volume of the saturated gas phase at mid-point conditions is given in column 8. The holdup ratio, (i.e. the ratio of column 6 to column 7), is given in column 9. The total pressure drop over the test section, expressed in terms of feet of water per foot of height, is given in column 10. The pressure drop regime[1,5] is shown in column 11.

Interpretation and Correlation of Results

Effect of Gas Phase Density on Flow Pattern

It has previously been shown[1,5] that the flow patterns occurring in the upward vertical flow of air-water mixtures are closely related to the pressure drop curve. In the earlier investigations, the flow was divided into four regimes, the boundaries of which were taken, by definition, as the volume ratios corresponding with the two minima and the maximum appearing in the pressure drop curve. It was also shown that the flow patterns observed were related to these arbitrarily-defined regimes.

The effect of a change in gas phase density is best illustrated by considering the pressure drop curves obtained with different gas phase densities at the same water velocity. Figure 1 shows the effect of gas phase density for a water velocity of 0.868 ft./sec. Multiple ordinate scales are employed on this figure to avoid overlapping of the curves. The curves shown in the figure illustrate the trend of the transition points to lower volume ratios with increasing density of the gas phase. Because of the interrelation between the flow patterns and the flow regimes previously demonstrated[1,5] this trend applies also to transitions from one flow pattern to another.

Correlations of the loci of the regime and flow pattern transitions are shown in Figures 2 to 4. Figure 2 indicates that the locus of the first minimum of the pressure drop curve (the transition between Regimes I and II) for all diameters and gas phase densities studied is represented fairly well by a single line on coordinates V_L and $R_v\rho^{1/3}D^{1/3}$. The dependence on tube diameter shown here is the same as has been noted previously.[5] The boundary lines between the different flow pattern regions are estimated from previous work. The locus of the second minimum of the pressure drop curve is correlated in Figure 4 where V_L is plotted against $R_v\rho^{1/3}D^{-2/3}$. The greater influence of tube diameter shown here as compared with previously published results[6] has arisen from a re-evaluation of the original data together with the results of additional experiments.

As can be seen in the lists of symbols accompanying each of these figures, much of the previously published data was used along with the new data in developing the correlations.

Effect of Gas Phase Density on Holdup

The overall effect of the density of the gas phase on the holdup curves is shown in Figure 5 for a superficial water velocity of 0.295 ft./sec. Multiple ordinates are employed on this figure also to avoid overlapping of the curves. The holdup decreases rapidly with increasing gas phase density at higher values of R_v and the maximum of the curve shifts to lower values of R_v. At lower values of R_v, in Regimes I and II, there is no

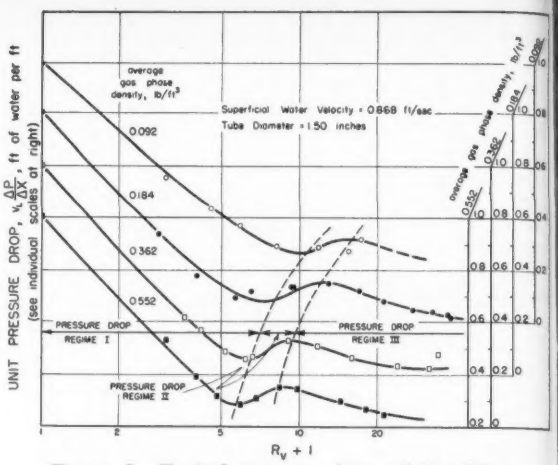
UNIT PRESSURE DROP, $v_L \frac{\Delta P}{\Delta X}$, ft of water per ft (see individual scales at right)
average gas phase density, lb/ft³
Superficial Water Velocity = 0.868 ft/sec
Tube Diameter = 1.50 inches
0.092
0.184
0.362
0.552
PRESSURE DROP REGIME I
PRESSURE DROP REGIME II
PRESSURE DROP REGIME III
$R_v + 1$

Figure 1—Typical pressure drop relationships.

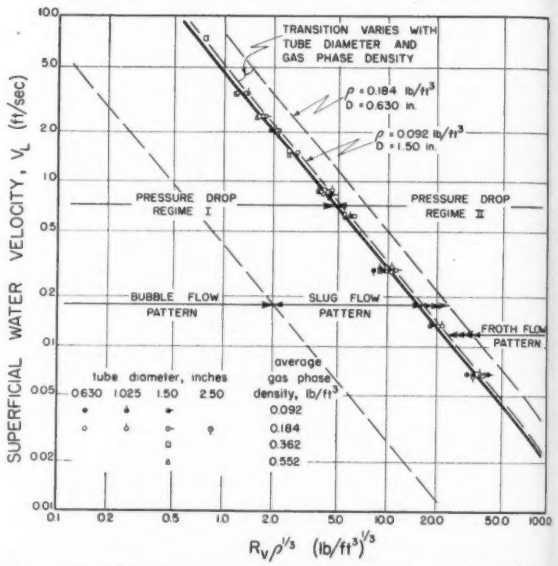
SUPERFICIAL WATER VELOCITY, V_L (ft/sec)
TRANSITION VARIES WITH TUBE DIAMETER AND GAS PHASE DENSITY
ρ = 0.184 lb/ft³ D = 0.630 in.
ρ = 0.092 lb/ft³ D = 1.50 in.
PRESSURE DROP REGIME I
PRESSURE DROP REGIME II
BUBBLE FLOW PATTERN
SLUG FLOW PATTERN
FROTH FLOW PATTERN
tube diameter, inches 0.630 1.025 1.50 2.50
average gas phase density, lb/ft³ 0.092 0.184 0.362 0.552
$R_v\rho^{1/3}$ (lb/ft³)$^{1/3}$

Figure 2—First pressure drop minimum locus (vs $R_v\rho^{1/3}$).

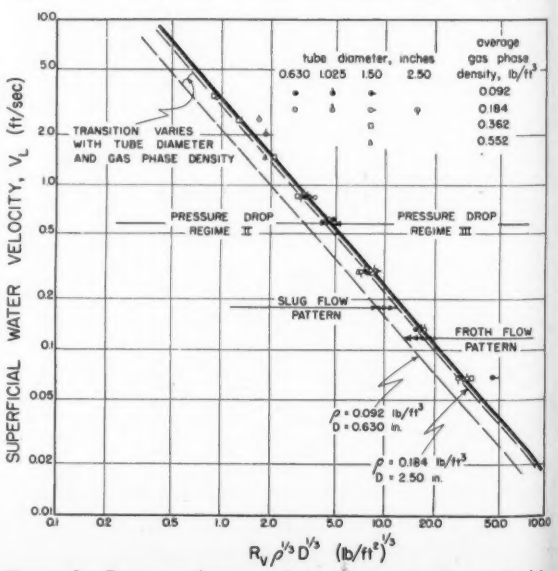
SUPERFICIAL WATER VELOCITY, V_L (ft/sec)
tube diameter, inches 0.630 1.025 1.50 2.50
average gas phase density, lb/ft³ 0.092 0.184 0.362 0.552
TRANSITION VARIES WITH TUBE DIAMETER AND GAS PHASE DENSITY
PRESSURE DROP REGIME II
PRESSURE DROP REGIME III
SLUG FLOW PATTERN
FROTH FLOW PATTERN
ρ = 0.092 lb/ft³ D = 0.630 in.
ρ = 0.184 lb/ft³ D = 2.50 in.
$R_v\rho^{1/3}D^{1/3}$ (lb/ft²)$^{1/3}$

Figure 3—Pressure drop maximum locus (vs $R_v\rho^{1/3}$ $D^{1/3}$).

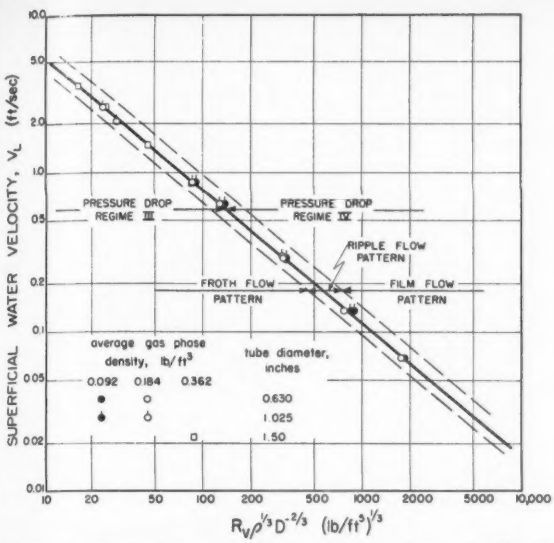

Figure 4—Second pressure drop minimum locus (vs $R_V\rho^{1/3}D^{-2/3}$).

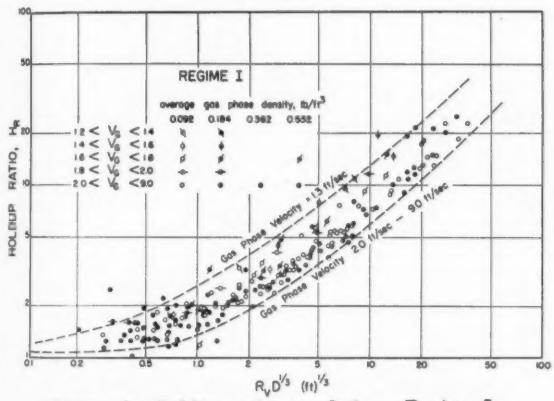
REGIME I
HOLDUP RATIO, H_R
average gas phase density, lb/ft³
0.092 0.184 0.362 0.552
Gas Phase Velocity = 1.3 ft/sec
Gas Phase Velocity 2.0 ft/sec – 9.0 ft/sec
$R_VD^{1/3}$ $(ft)^{1/3}$

Figure 6—Holdup ratio correlation—Regime I.

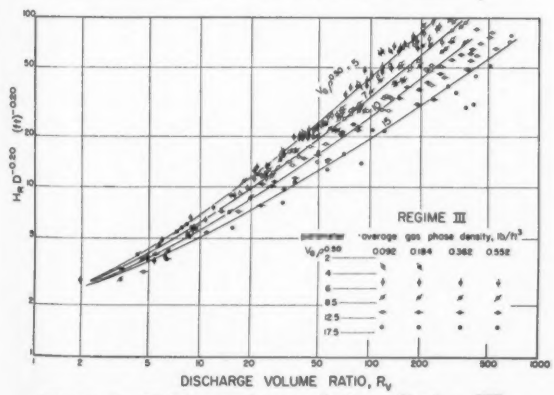

Figure 8—Holdup ratio correlation—Regime III.

apparent effect of gas phase density. The holdup data have been correlated separately for each regime.

Figure 6 shows the correlation of the holdup ratio for Regime I. The data form a broad band but show a segregation based upon superficial gas phase velocity. The upper portion of the band includes the bulk of the data at superficial gas phase velocities below 1.7 ft./sec. (lower limit of data is 1.3 ft./sec.). The data for gas phase velocities of 2.0 ft./sec. and higher lie in the lower part of the band.

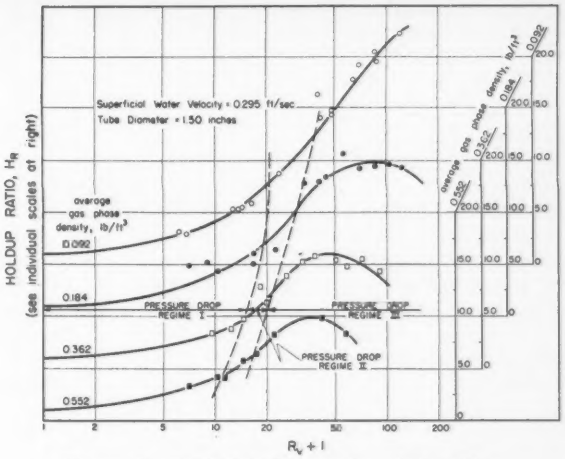

Figure 5—Typical holdup ratio relationships.

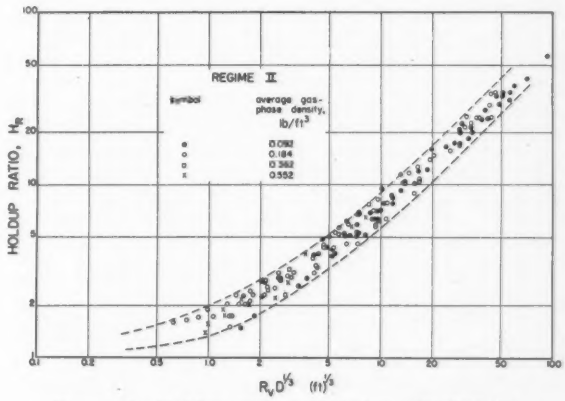

Figure 7—Holdup ratio correlation—Regime II.

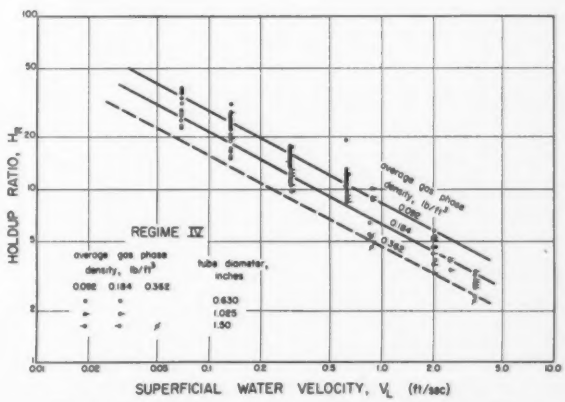

Figure 9—Holdup ratio correlation—Regime IV.

In Regime II also the holdup ratio falls within fairly well defined limits when plotted against $R_VD^{1/3}$. The data, which are shown in Figure 7, exhibit little systematic scattering. The holdup ratio is not affected significantly by the gas phase density in either Regime I or Regime II.

The gas phase density does have an effect on the holdup ratio in Regimes III and IV however. Figure 8 shows the correlation for Regime III with $H_RD^{-0.20}$ plotted against R_V with parameter $V_G\rho^{0.50}$. The correlation of the holdup ratio in Regime IV is shown in Figure 9. These data indicate that, at constant superficial water velocity, H_R is inversely proportional to $\rho^{0.43}$.

Effect of Gas Phase Density on Pressure Drop

The friction factor is obtained from the observed pressure drop through Equations (1) and (2) previously reported.[5] As was found for the data at a mid-point pressure of 36.0 p.s.i.a., fairly good correlation is obtained if the friction factor is plotted against DV_L with a parameter of $D^{0.5}V_G$ as shown in Figure 10. The abscissa is proportional to the superficial Reynolds Number of the water since the density and viscosity of the water are essentially the same for all tests.

In the development of the correlation shown in Figure 10, all of the data for the air-water system were considered, including the results previously presented.[1,5] The points shown on the figure are representative of the complete range of variables on which the correlation is based, and are not solely from the present investigation. The number appended to each point is the experimental value of the parameter, $V_G D^{0.5}$, for the point. The data show that the density of the gas phase has no significant effect on the friction factor. The analysis of the additional data, however, has resulted in some minor adjustments in the chart previously presented.[5] It should also be noted that the dependence of the friction factor on tube diameter has now been confirmed for a gas phase density of 0.092 lb./ft.^{3}, the original determination having been made for a gas phase density of 0.184 lb./ft.^{3}. The conventional single phase friction factor has been included in Figure 10 as the curve for a parameter value of zero. The dashed lines shown for low parameter values are approximate only and were obtained by interpolation.

While the data used to develop this correlation covered the four flow regimes, it was not possible to get equally good representation in all of these. The correlation shown in Figure 10 is applicable to flow in the first three regimes but gives low values of friction factor in Regime IV. The use of the correlation in Regime IV is not recommended.

Conclusions

The correlation presented in this paper should permit the prediction of flow pattern, holdup and pressure drop for the flow of immiscible gas and liquid water phases with average gas phase densities in the range 0.092 lb./ft.^{3} – 0.552 lb./ft.^{3} and tube diameters from 0.5 to 3.0 inches. The correlations are restricted to cases in which the fractional change in gas density is small enough to justify the use of an average value.

Nomenclature

D = tube diameter, ft.

f'_L = superficial friction factor = $\dfrac{g_c D}{2V_L^2}\left(\dfrac{\Delta F}{\Delta X}\right)_L$

$\left(\dfrac{\Delta F}{\Delta X}\right)_L$ = irreversibility effect, feet of water per foot of height.

g_c = dimensional conversion factor, lb.$_M$ ft./lb.$_F$sec.^{2}

G = flow rate of gas phase, lb./hr.

L = flow rate of water, lb./hr.

ΔP = pressure drop, lb./ft.^{2}

R_v = volume ratio of gas phase to water, Gv_G/Lv_L

v_L = specific volume of water, ft.^{3}/lb.

v_G = specific volume of gas phase, ft.^{3}/lb.

V_L = superficial water velocity based upon the total tube cross-section, ft./sec.

V_G = superficial gas phase velocity based upon the total tube cross-section, ft./sec.

ΔX = incremental height, ft.

ρ = density of gas phase = $\dfrac{1}{v_G}$, lb./ft.^{3}

References

(1) Govier, G. W., Radford, B. A., and Dunn, J. S. C., C.J.Ch.E., **35**, 58 (1957).

(2) Bennett, J. A. R., Atomic Energy Research Establishment AERE CE/R 2497 (1958).

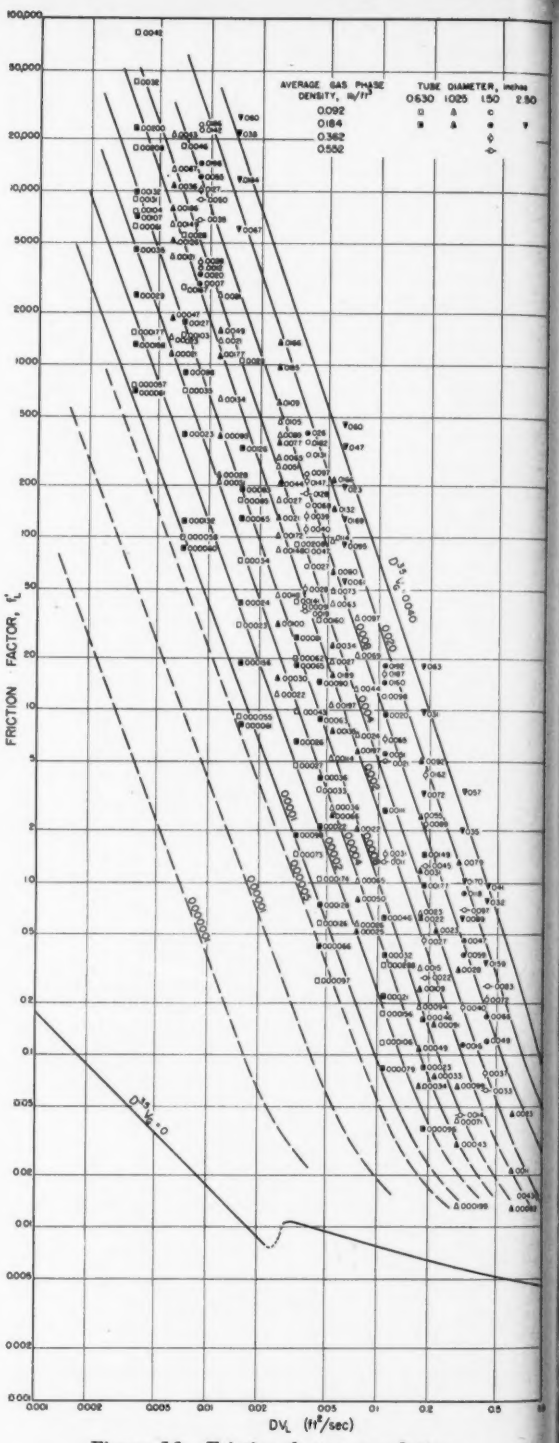

Figure 10—Friction factor correlation.

(3) Isbin, H. S., Moen, R. H., and Mosher, D. R., United States Atomic Energy Commission AECU-2994 (November 1954).

(4) Calvert, S., and Williams, B., A.I.Ch.E. Journal, **1**, 7 (1955).

(5) Govier, G. W., and Short, W. Leigh, C.J.Ch.E., **36**, 19 (1958).

(6) Sullivan, G. A., M.Sc. Thesis, University of Alberta (1958).

* * *